

The Analysis of Factors Influencing Nanoparticle Uptake in Primary Cells

Pooja Pushparaj

Master of Engineering

Department of Bioengineering
McGill University
Montreal, Quebec, Canada

August 2018

A thesis submitted to McGill University in partial
fulfillment of the requirements of the degree of
Master of Engineering

© Pooja Pushparaj, 2018

Abstract

There have been burgeoning developments in nanoparticle (NP) research for biomedical applications and nanomedicine. However, very few NPs have made it to clinical trials, and even fewer have reached clinical practice. This wide disparity between bench discoveries and their effective clinical translation is mainly due to insufficient knowledge of the nano-bio interface. We believe that there are multiple factors in the *in vitro* environment that are overlooked leading to misinterpretation of data that is collected.

Recently, several studies have been performed to diminish the aforementioned gap aimed at achieving a more in-depth understanding of the biological identity of NPs and their inherent cytotoxic properties. However, there is still a dearth in significant research in this field. Therefore, the main objective of my thesis is to study the factors that affect the cellular uptake of nanoparticles (NPs) which include both physical and biological influences. Uptake trends and the associated factors were studied in primary fibroblasts derived from the salivary glands of adult male and female human donors and primary tumor and stromal cells of patients from different stages of cancer progression. We aim to document the roles played by gender, disease progression and other factors in the nanobio interface in NP endocytosis and thus their effects on potential clinical applications of NPs and personalized medicine.

Abrégé

Il y a eu des développements en plein essor dans la recherche sur les nanoparticules (NP) pour les applications biomédicales et la nanomédecine. Cependant, très peu d'IP ont réussi à faire des essais cliniques, et encore moins ont atteint la pratique clinique. Cette grande disparité entre les découvertes au banc et leur traduction clinique efficace est principalement due à une connaissance insuffisante de l'interface nanobio. Nous pensons que plusieurs facteurs de l'environnement in vitro sont ignorés, ce qui conduit à une mauvaise interprétation des données collectées.

Récemment, plusieurs études ont été réalisées pour réduire l'écart susmentionné visant à mieux comprendre l'identité biologique des NP et leurs propriétés cytotoxiques inhérentes. Cependant, les recherches importantes dans ce domaine sont encore insuffisantes. Par conséquent, l'objectif principal de ma thèse est d'étudier les facteurs qui affectent l'absorption cellulaire des nanoparticules (NP), notamment les influences physiques et biologiques. Les tendances de l'absorption et les facteurs associés ont été étudiés dans les fibroblastes primaires dérivés des glandes salivaires de donneurs humains mâles et femelles adultes et les tumeurs primitives et les cellules stromales des patients à différents stades de la progression du cancer. Nous visons à documenter les rôles joués par le sexe, la progression de la maladie et d'autres facteurs dans l'interface nanobio dans l'endocytose des NP et donc leurs effets sur les applications cliniques potentielles des NP et de la médecine personnalisée.

Preface and Author Contributions

Chapter 1 of the thesis has been adapted from a review article manuscript co-authored by Pooja Pushparaj and Santiago Gutiérrez Restrepo. Portions of the text and figures in Chapters 3 to 6 has been published in the student's co-first authored paper titled 'Effect of Cell Sex on Uptake of Nanoparticles: The Overlooked Factor at the Nanobio Interface' and adapted with permission from Serpooshan V, et al. Effect of Cell Sex on Uptake of nanoparticles: the overlooked factor at the nanobio interface. ACS Nano. 2018;12:2253–2266. Copyright 2018 American Chemical Society (Copyright Clearance enclosed).

Only experiments conducted at McGill University has been included in the experimental data and analysis. All Transmission Electron Microscopy experiments and analysis in Chapters 5 and 6 were conducted at the Facility for Electron Microscopy Research, McGill University by Dr. Sara Sheibani, Prof. John Presley, and Prof. Hojatollah Vali. Flow cytometry experiments in the Cell Gender project were conducted by Joyce Jang at the Meakins Christie Laboratories, McGill University Health Center. All experiments in the Cancer Nanoparticle project was performed together by Pooja Pushparaj and Santiago Gutiérrez Restrepo. All other material is the original, unpublished, work by the author, Pooja Pushparaj.

Acknowledgements

I would like to start off by emphasizing that this project is the amalgamation of revolutionary ideas from our many collaborators, advisors, and individuals who provided valuable inputs at every stage of the project. I unequivocally thank each and every one of them. I would like to express my deepest appreciation for my Supervisor Prof. Joseph “Matt” Kinsella for his expert guidance and support throughout my Masters without which this project would never have been a reality. My gratitude goes out to all members at Kinsella lab, Jose Gil Munguia-Lopez, Tao Jiang, Salvador Flores Torres, and Jacqueline Kort Mascort, for their advice, assistance and encouragement. One couldn't have asked for a better bunch of lab mates.

With the deepest regard, I acknowledge the contributions of all our collaborators. I extend my sincere gratitude to Prof. Morteza Mahmoudi, Harvard Medical School, for giving me the opportunity to collaborate in his ambitious project on ‘Cell Gender’ and for all the guidance he provided me throughout. I would also like to thank André Charbonneau and Prof. Simon Tran for providing the cells for the cell gender project. My heartfelt appreciation goes out to the members at the Facility for Electron Microscopy Research, McGill University, namely Dr. Sara Sheibani, Prof. Hojatollah Vali, Prof. John Presley, Kelly Sears, Kaustuv Basu, and Jeannie Mui for their assistance with the TEM data. I would also like to express my sincere gratitude to all authors of the research article based on this project

published in ACS Nano namely, Vahid Serpooshan, Michal Wojcik, Albert Y. Jang, Michelle R. Santoso, Haina Huang, Reihaneh Safavi-Sohi, Niloofar Haghjoo, Hossein Nejadnik, Haniyeh Aghaverdi, Ke Xu, and Phillip Chung-Ming Yan. For the ‘Cancer Nanoparticle’ project, I am indebted to Prof. Veena Sangwan, Prof. Morag Park and other collaborators who have given valuable inputs in terms of experimental materials and advice.

My acknowledgements would be incomplete without thanking the support provided by members of staff, fellow students, research assistants, and technicians in the collection of materials and data, the design and construction of apparatus, and the performance of experiments. My sincere gratitude goes out to Joyce Jang for helping out with flow cytometry experiments and data analysis, Denis Flipo for assistance with cell sorting, flow cytometry and confocal imaging at UQAM, Galyna Shul from NanoQAM for nanoparticle characterization studies. My heartfelt gratitude goes out to Prof. Adam Hendricks, Sofia Cruz Tetlalmatzi, and Abdullah Chaudhary for help with materials, instruments, and guidance for STORM imaging. I also acknowledge the contributions of Kurt Dejgaard at the LC-MS/MS facility at McGill and Hong Zhao at the Rosalind & Morris Goodman Cancer Center.

Intense research environments can be intimidating at times. Thus, it is inevitable to appreciate everyone who contributes in making student life slightly more bearable. I am indebted to my lab mate Santiago Gutiérrez Restrepo for managing my lab work during my thesis writing phase. I thank Nirmal Kanagasabai for being a constant pillar of support and for all the advice with the thesis structure and technical assistance with LaTeX. I thank Preeti Bhatt, Sonali Uttam, Rohan Mahimkar, and all my other friends who have always inspired me on with their love and care.

Finally, I cannot stress enough how important the love and support from my parents has been in showing me the way out of every stumbling block in the course of my graduate studies. I am indebted to my mother, father and brother for this and above all, God Almighty for showering his blessings on me and giving me the strength to face adversities and emerge victorious.

Contents

1	Introduction and Literature Review	1
1.1	Nanomedicine and Precision Nanomedicine	2
1.2	Research at the Nano-Bio Interface	3
1.3	Nanoparticles and the Protein Corona	4
1.4	Cellular Endocytosis of Nanoparticles	5
1.5	Sex Differences in Life Science Research	7
1.5.1	The origin of cell sex	8
1.5.2	Cytoskeletal Differences among Cells	10
1.6	Other Uptake Determinants: Cancer Progression	11
2	Background and Thesis Overview	13
2.1	Description of Experimental Concepts	13
2.1.1	Flow Cytometry	14
2.1.2	Confocal Microscopy	14
2.1.3	Stochastic Optical Reconstruction Microscopy (STORM)	15
2.1.4	Liquid Chromatography Tandem Mass Spectrometry (LC-MS/MS)	15
2.1.5	Transmission Electron Microscopy (TEM)	15
2.1.6	Patient-derived Xenograft (PDX) Tumor Models	16
2.2	Factors Involved in Cell Nanoparticle Uptake	16
2.2.1	Patient and Disease-related Factors	16
2.2.2	Environmental Factors	17
2.3	Thesis Overview	17
2.3.1	Advantages of using Primary Cells over Cell Lines	18
2.3.2	Research Aims & Hypothesis	18
2.3.2.1	Cell Gender Project	19
2.3.2.2	Cancer Nanoparticle Project	19
3	Methodology	20

3.1	Cell Gender Project	20
3.1.1	Materials	22
3.1.2	Methods	22
3.1.2.1	Cell Isolation and Culture	22
3.1.2.2	Flow Cytometry	23
3.1.2.3	Confocal Imaging	23
3.1.2.4	Confocal Image Analysis	23
3.1.2.5	Transmission Electron Microscopy (TEM)	24
3.1.2.6	Zeta Potential Analysis	24
3.1.2.7	Fluorescence Labeling for STORM Imaging	24
3.1.2.8	STORM Imaging	25
3.1.2.9	Liquid Chromatography Tandem Mass Spectrometry (LC-MS/MS)	26
3.2	Cancer Nanoparticle Project	27
3.2.1	Materials	28
3.2.2	Methods	29
3.2.2.1	Nanoparticle Characterization	29
3.2.2.2	Cell Sorting	29
3.2.2.3	Nanoparticle Uptake Studies	29
3.2.2.4	Flow Cytometry	29
3.2.2.5	Confocal Microscopy	30
4	Nanoparticle Uptake Studies	31
4.1	Cell Gender Project	31
4.1.1	Flow Cytometry	31
4.1.2	Confocal Imaging	32
4.1.2.1	Confocal Image Analysis	35
4.2	Cancer Nanoparticle Project	35
4.2.1	Nanoparticle Characterization	35
4.2.2	Flow Cytometry	36
4.2.3	Confocal Imaging	37
5	Uptake Variation Analysis Studies	40
5.1	Cytoskeletal Analysis	40
5.1.1	Super-Resolution Microscopy (STORM)	41

5.1.1.1	Actin Imaging	41
5.1.1.2	Clathrin Imaging	41
5.1.2	Transmission Electron Microscopy (TEM)	44
5.2	Zeta Potential & Proteomic Analysis of QD Corona	46
5.2.1	Zeta Potential Analysis	47
5.2.2	Liquid Chromatography Tandem Mass Spectrometry (LC-MS/MS)	47
6	Discussions and Conclusion	50
6.1	Discussions	50
6.1.1	Flow Cytometry	50
6.1.2	Confocal Microscopy	52
6.1.3	Super Resolution Microscopy	52
6.1.4	Transmission Electron Microscopy	53
6.1.5	Zeta Potential Analysis and Proteomics	54
6.1.6	Cell Gender Project: Collaborator's Work	57
6.2	Conclusions and Future Work	58
	List of Publications	60
	Bibliography	61

List of Figures

1.1	Pathways of entry into the cell. An increasing number of endocytic pathways are being defined, each mechanistically distinct and highly regulated at the molecular level. These pathways facilitate cellular signaling and cargo transport. Controlling the route of nanoparticle uptake is important for both mediating their intracellular fate as well as their biological response. [Republished with permission of Royal Society of Chemistry, from Strategies for the intracellular delivery of nanoparticles, L.Y.T. Chou, K. Ming, W.C.W. Chan, 40, 2011; permission conveyed through Copyright Clearance Center, Inc.]	6
3.1	Overview of methodology followed for nanoparticle uptake studies and analysis in human salivary gland fibroblasts from 43-year-old male and 45-year-old female patients	21
3.2	Overview of the nanoparticle cancer project.	27
4.1	Flow cytometry plots showing quantum dot uptake by single-population male and female salivary gland fibroblasts. (A) depicts the percent cell count for each group for three repeats denoted by solid circles (females) and squares (males). The same data is shown in the form of mean fluorescence intensity (MFI) in (B). Two asterisks (**) indicates a p-value lesser than 0.01	32
4.2	Flow cytometry plots showing quantum dot uptake by co-culture of male and female salivary gland fibroblasts. (A) depicts the percent cell count for each group for three repeats denoted by solid circles (females) and squares (males). The same data is shown in the form of mean fluorescence intensity in (B). Four asterisks in (A) denote a high statistical significance of p-value < 0.0001.	33
4.3	Quantum dot uptake histograms for the co-culture experiment showing absolute uptake cell count in red for unlabeled population, female population in blue and male population in orange.	33
4.4	Confocal images of QD treated salivary gland fibroblasts from a 48 year old male (A) versus a 45 year old female patient (B) and a 74 year old male (C) versus a 77 year old female patient (D). (Red - Plasma Membrane, green - QDs, blue - DAPI). White arrows show green areas where QDs have accumulated. Scale bar is $50 * 10^{-6}m$	34
4.5	Percentage of QD uptake from each gender group quantified using confocal images and ImageJ. Male cells from both age-matched groups (A - 48 year old male and 45 year old female; B - 77 year old male and 74 year old female) internalize more QDs. . .	35
4.6	Mean Fluorescence Intensity of NP - treated samples measured via flow cytometry. . .	36
4.7	Percentage of cells for each type that endocytosed nanoparticles.	36

4.8	: Confocal images of nanoparticle - treated cells extracted from 136T tumors. The cell membrane is labeled in green, nucleus with DAPI (blue), and nanoparticles in red. Panels A2, B2, and C2 show nanoparticle accumulation in the cells. Scale bar is $33 * 10^{-6}m$	38
4.9	Confocal images of nanoparticle - treated cells extracted from 181T tumors. The cell membrane is labeled in green, nucleus with DAPI (blue), and nanoparticles in red. Panels A2, B2, and C2 show nanoparticle accumulation in the cells. Scale bar is $20 * 10^{-6}m$	39
5.1	Super resolution images showing differences between organization, distribution and morphology of actin filaments or bundles in salivary gland primary fibroblasts extracted from the male (A, B) versus female (C, D) patients. Scale bar is $1 * 10^{-6}m$	42
5.2	Super resolution images showing the arrangement of clathrin heavy chains in both female (a to c) and male (d to f) cells before and after incubations with QDs. Red circles in male treated cells indicate localization of clathrin to coated pits. Scale bar is $1 * 10^{-6}m$	43
5.3	TEM images of salivary gland female (A, B) and male (C, D) control fibroblast cells. The female cells exhibit a dense network of filaments throughout the cells and a bundle of stress fibers close to the cell surface (arrow at the top of A). The male cells have much fewer filaments within the cells. Microtubules are more abundant in the male cells compared to the female.	45
5.4	TEM images showing 10 nm gold NPs. Gold NPs can be seen within the cytoplasm of a salivary gland male fibroblast cell (A). White arrows point to gold particles. A1 is a close up of the gold aggregates, and A2 shows the same particle under overfocused conditions. (B) Inclusion of gold NPs in the lysosome. B1 is a close up showing an individual gold particle.	45
5.5	TEM images showing the presence of clathrin coated (A) and caveolae (B) vesicles in a salivary gland male fibroblast cell. There are no gold NPs present inside any of these vesicles. Some of the clathrin coated vesicles contain some gold particles on the outer surface (inset A1 in A).	46
5.6	TEM images of the salivary gland female fibroblast cell revealing the linear alignment of coated vesicles along stress fibers in agreement with the super-resolution images	47
5.7	Graph showing normalized spectral counts of secreted proteins identified in the male, female and co culture protein coronas.	49
6.1	Forward and side scatter characteristics of a typical flow run of NP-treated t136T and f136T gastric cells.	51

List of Tables

3.1	Cells in Cancer NP Project	28
5.1	Table showing zeta potential values of QDs both before and after conditioning with cell supernatants from male, female and co culture samples	47
6.1	The secreted proteins identified from the hard corona of cell samples. Mean abundance is the average of the percentage normalized spectral counts of the proteins in the male, female and co-culture coronas. Net charge for each protein is given at physiological pH=7.4.	55

1

Introduction and Literature Review

Nanotechnology, the manipulation of material at the nanoscale, is a science that has garnered a great deal of interest since the past few decades owing to the distinctive properties of nanomaterials that make them suitable for several applications in bioengineering and biomedical engineering, semiconductor industries, cosmetics, microfabrication, clothing, and the electronics industry [1]. In particular, nanomedicinal research has been thriving in the previous years. Despite these advancements, it is yet to make a mark in clinical translations and other applications because of challenges that come up in terms of its toxicity, environmental impact and a lack of understanding of events at the interface between the NPs themselves and the physiological environment, also called as the nano-bio interface [2, 3, 4]. The *nano-bio interface* comprises the dynamic physicochemical interactions, kinetics and thermodynamic exchanges between nanomaterial surfaces and the surfaces of biological components (for example proteins, membranes, phospholipids, endocytic vesicles, organelles, DNA and biological fluids) [5]. The following sections will give an overview of some basic concepts and trends in nanomedicinal research along with a review of major studies in the literature related to the background and hypothesis of this thesis project.

1.1 Nanomedicine and Precision Nanomedicine

Nanomedicine is a fast-growing domain mainly concerning the application of nanotechnology for the diagnosis, treatment, and prevention of diseases. This field promises groundbreaking tools in clinical research. As is evident from the name, nanomedicine involves the use of nanomaterials or particles with dimensions of nanometer scale in diagnostic devices [6], contrast agents [7], biosensors [8], tissue engineering applications [9], drug delivery [10], analytical tools [11], and many more innovative uses. Due to the similarity of their size to biological molecules, nanomaterials are integral in biomedical research. Nanomaterials may also be functionalized to make them more biocompatible for their respective targets.

Nanomedicine helps overcome many of the limitations associated with traditional drug treatments. Traditional drugs may have low water solubility making it difficult for the body tissue to absorb it. Sometimes these drugs have low lifetimes in the body and are quickly excreted before it has the time to exert its full pharmaceutical effect. Some drugs may cause adverse side effects to healthy tissues and organs. Nanomedicine wipes out all these disadvantages in lower dosages and time when compared to its traditional counterpart [12].

In 2015, the sales for nanomedicinal products reached \$16 billion. New nanotechnology research is being globally funded with an increase of 45% per year with product sales exceeding \$1 trillion as of 2013 [13].

Mounting evidence is now coming to light that treatment strategies devised for the average person does not necessarily elucidate the same response from every individual. For example, the same drug may cause different effects on male and female patients [14]. The concept of precision medicine involves tailoring novel healthcare strategies according to the patient's genetic makeup, his lifestyle, and environmental conditions. It encompasses individual modification of products, medical decisions, practices, diagnosis, and treatment strategies to achieve the best possible result for each patient. Vari-

1.2 Research at the Nano-Bio Interface

ous analytical tools, cellular assays, molecular diagnostics, and imaging are employed to formulate the best suited medical model for a patient [15].

Precision medicine is gaining even more relevance in the era of sex-dependent differences in clinical and biomedical research. Here, we would like to introduce a relatively new term, '*precision nanomedicine*', which incorporates customization of nanomedicinal techniques to match the genes, lifestyle and environmental characteristics for each individual patient. The quadrugnostic NPs is one such technique that could achieve a precise diagnostic localization of tumors and facilitate personalized drug treatment [16]. Genetic variation, being the defining characteristic of cancer, makes the disease one of the most common target applications of precision nanomedicine with individualized tumor diagnostics and tailoring of precise nanodrug treatments taking the research in cancer biology by storm [17].

Using precision nanomedicine, we can target nanomedicinal therapies to very narrow sites of affected tissues and minimize adverse effects to the rest of the body. Nanotechnology has the potential to actually reduce dosage frequencies and quantities of medications. Scientists have been successful in designing slow release nanotherapeutics which can be injected or implanted into the body at a suitable site. The biodegradable nanoparticle itself breaks down into naturally occurring substances and is eliminated from the body without any hassles [18].

1.2 Research at the Nano-Bio Interface

When a nanoparticle interacts with various components of the biological environment, it gives rise to a myriad of dynamic biophysicochemical reactions. These reactions affect the biological identity of the nanoparticles and their subsequent fate in the biological environment due to a number of resultant phenomena like the formation of protein coronas, particle wrapping, intracellular uptake, and biocatalytic processes [2]. The modification of NP biological identity from its laboratory-designed version can potentially reduce the expected drug targeting yield, drug release profile, and therapeutic efficiency

1.3 Nanoparticles and the Protein Corona

[4]. These events along with the properties of the nanoparticles themselves such as surface functionalization, size, roughness, shape, natural surface chemistry, etc. allow one to predict their course of action on introduction into a physiological environment.

One of the most important advances for nanomedicinal research, which is now being researched upon with great gusto, is the clear understanding of what happens at the cell-nanoparticle interface. While protein adsorption onto planar surfaces has been investigated for decades, detailed studies of NP-protein interactions have only started recently [4]. Protein-protein interactions can help in surface modification of nanoparticles with proteins, thereby, recruiting specific proteins from the plasma in order to enhance targeting [19]. Mahmoudi and co-workers also support the use of zwitterions as ideal coatings for corona-free NPs with high therapeutic efficacy [20].

Research at the nano-bio interface is developing in leaps and bounds. However, it is needless to say that much more resources in nanotechnology research should be allocated towards this sector in order to bridge the gap between laboratory research and clinical translation of nanomedicine.

1.3 Nanoparticles and the Protein Corona

Regarding the engineering of treatments for the most common diseases today, one of the focal points of research is nanoparticle-based treatments. Different types of cancers, autoimmune diseases, diabetes and even cardiovascular diseases [21, 22] have a potential treatment related to nanoparticles or nanocarriers due to advantages such as elevated drug targeting efficiency, lower toxicity and increase in absorption by encapsulation of agents [23] together with properties of size, charge, magnetism, etc.

Prabhakar, et al. [24] first reported enhanced permeability and retention effect, a characteristic of effective accumulation of nanoparticles in solid tumors with a particle size between 50 and 200 nm. However, there are several factors that may influence this effect like the presence of conductive systems, type, location and size of the tumor, and the phagocytic cell activity related to sex, age, type of treatment [25]. Differences in these factors impart relevance to the research of a more tailored treatment

1.4 Cellular Endocytosis of Nanoparticles

for individuals.

Recent studies about how nanoparticles are dispersed in the body and are subsequently taken up by the cells showed that there is a protein corona formation on the surface of each particle. This corona is divided in two regions: the inner part, also called ‘hard’ corona, that adheres to the nanoparticle rapidly, and the outermost part or the ‘soft’ corona which is more unstable and varies considerably in composition depending on the environment [26].

The protein corona has an effect not only on the cellular uptake of the nanoparticle, but in the whole biological behavior of it, including its toxicity, pharmacokinetics and cellular trafficking. The understanding of the formation of protein corona is crucial in order to improve the therapeutic effect of a nanoparticle-based treatment. However, recent findings suggest that corona conformation and composition vary under several conditions, such as patient health and/or disease specifications, or even factors such as age, sex, medical history, and ethnicity [27]. New approaches such as pre-coating of NPs with proteins may help in the formation of a more desirable ‘hard’ corona [28], creating a liposome with a dynamic protein corona system that can cross through the body and accumulate in tumor sites [29]. New understandings about a personalized protein corona for different diseases have also been identified [30].

1.4 Cellular Endocytosis of Nanoparticles

The plasma membrane of the cell maintains a homeostatic environment within it with the help of its highly selective permeable nature by allowing only certain ions, organic molecules, and the like to enter the cell. The molecules that cross this selective barrier range in size from sub-nanometer (ions) to tens of nanometers (proteins) in size which is the same size range as that of nanoparticles. As a nanoparticle approaches the cell surface, it encounters a layer of negatively charged oligosaccharides consisting of glycoproteins and glycolipids in the plasma membrane. The cell type [31] as well as the physicochemical properties of the nanoparticle like size [32], shape [33], and surface chemistry [34]

1.4 Cellular Endocytosis of Nanoparticles

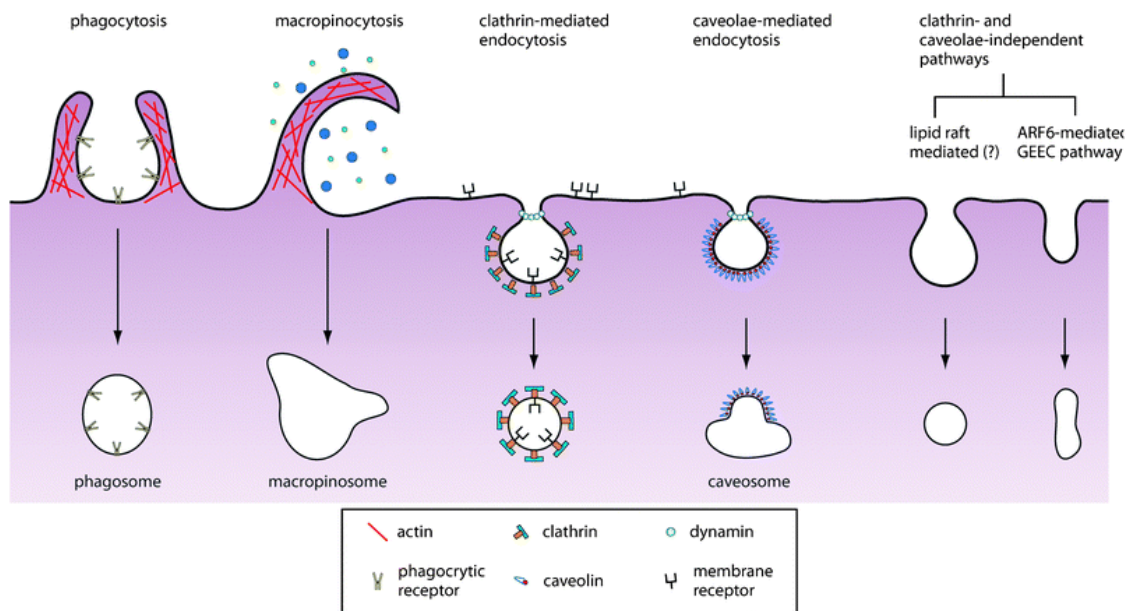


Figure 1.1: Pathways of entry into the cell. An increasing number of endocytic pathways are being defined, each mechanistically distinct and highly regulated at the molecular level. These pathways facilitate cellular signaling and cargo transport. Controlling the route of nanoparticle uptake is important for both mediating their intracellular fate as well as their biological response. [Republished with permission of Royal Society of Chemistry, from Strategies for the intracellular delivery of nanoparticles, L.Y.T. Chou, K. Ming, W.C.W. Chan, 40, 2011; permission conveyed through Copyright Clearance Center, Inc.]

affect the endocytosis pathway that the NP would follow to gain entry into the cell [26].

Cellular internalization of particles involves the generation of membrane-enclosed vesicles from the plasma membrane enclosing the particle of interest to be endocytosed. Depending on the size and surface chemistry of these particles, they may enter cells via different mechanisms (see 1.1). One such mechanism is pinocytosis characterized by invagination of the plasma membrane to bring particles suspended in extracellular fluid into the cell. Pinocytosis may be further classified into macropinocytosis, clathrin-mediated endocytosis, caveolin-mediated endocytosis and clathrin- and caveolin-independent endocytosis [35]. Micrometer-sized particles usually enter the cell through phagocytosis or macropinocytosis [36]. In clathrin-mediated endocytosis, receptor–ligand binding triggers the recruitment and formation of “coated pits” (clathrin) on the cytosolic side of the plasma membrane. The pits self-assemble into closed polygonal cages that facilitate the endocytosis. Clathrin assembly is also responsible for the

1.5 Sex Differences in Life Science Research

formation of vesicle necking and the pinch-off process in the late stage of membrane wrapping of NPs. Caveolin-dependent endocytosis, on the other hand, results in the formation of a flask-shaped rafts (caveolae), approximately 50-80 nm in diameter, on the cytoplasmic side of the cell membrane. For large NPs or for those that are not conjugated with any ligands, endocytosis may occur via transmembrane penetration or non-specific interactions [37].

Numerous studies in the past have brought the dominance of clathrin-mediated endocytosis pathway in cells as the mechanism preferred by nanoparticles [38, 39, 40]. In this pathway, cytosolic protein clathrin-1 polymerizes on the cytosolic side of the cell membrane as a result of nanoparticle-receptor interactions [41]. This protein proceeds to wrap the nanoparticles inside the vesicle which subsequently buds off with the help of GTPase activity of dynamin giving rise to clathrin-coated vesicles [42]. These coated vesicles move towards the interior regions of the cell regulated by the cell cytoskeleton. The clathrin coat of the vesicles is then shed off in the cytosol [43].

Having been introduced to the major concepts underlining this thesis, we will now proceed to discuss factors like sex differences and disease progression and their association with the aforementioned phenomena at the nano-bio interface.

1.5 Sex Differences in Life Science Research

When choosing a treatment for a disease a variety of factors are usually reviewed, including age, lifestyle, drug effects, pregnancy, and medical history among others. However, sex is of the most novel interest when it comes to tailoring therapies for individual patient diseases [44]. Sex precision medicine aims to consider physiological differences between male and female animals, tissues, and cells, to improve the accuracy and effectiveness of drugs. Since different areas of research have not come to a conclusion about these sex differences due to a lack of use of an equivalent representation of female subjects as males in experimental studies, it is very important to clearly state which differences are commonly found in each medical condition [45].

1.5 Sex Differences in Life Science Research

Sex differences have been studied in several health fields that try to explain variations in disease patterns. Sex-evident differences are related to underlying biological pathways, sex hormones, behavioral factors, etc. [46]. In the case of diabetes, some interesting data have so far been collected. Mauvius et al. showed that even though global diabetes prevalence is higher in men, there are more women with diabetes than men. Specifically, the prevalence of men suffering from diabetes before puberty is higher, but there are more diabetic post-menopausal women [47].

Also, evidence demonstrates that sex has a significant influence on the development of autoimmune diseases, especially in the ability to protect cells from damage; it is thought that because of the cytoprotective properties of estrogen, females generally have greater resistance [48]. According to other studies, diseases like cutaneous melanoma are more likely to develop in men (1 in 58) than in women (1 in 82). Sex steroids may play an important role as malignant melanoma is rare before puberty in females but sharply increases from puberty until menopause [49].

1.5.1 The origin of cell sex

Referring specifically to cells, it took some time to study the non-obvious differences between male and female cells. For a long time, it was considered that apart from gametes, all cells were asexual. Sex chromosomes were considered to have a direct effect only in reproductive organ development and function. However, some studies demonstrate that they are involved in many cellular functions unrelated to reproduction and every cell in the body is either male or female [50]. Functions like production of nitric oxide, secretion of extracellular matrix, regulation of cellular pathways associated with apoptosis and cell survival, mitochondrial energy metabolism, etc., are modulated by sex steroids and may impact the patient's recovery or treatment [46].

Early studies show preliminary information regarding cell sex differences. For example, female cells show more sensitivity to some cytotoxic reagents than males. In most of these studies, the hormonal factor was eliminated by using embryonic cells and the observed behavior was governed by the

1.5 Sex Differences in Life Science Research

sex chromosomes alone [51].

Sex differences have been observed in the paracrine function of mesenchymal stem cells (MSCs). Zeller and coworkers [52] studied myocardial recovery after ischaemic reperfusion in rats with the hypothesis that female MSCs from the heart would improve myocardial recovery as compared to male MSCs after ischemia-reperfusion injury. Their studies showed that ablation of tumor necrosis factor receptor 1 (TNFR1) increases protective growth factor production in male rats but not in female rats. This deficiency of TNFR1 increased the degree of myocardial recovery associated with male MSCs proving that female stem cells produce lower proinflammatory cytokines and higher growth factor levels compared with their male counterparts.

There have been several studies on sex-based paracrine differences in humans. Serpooshan, et al., [53] observed significant variations in the production of 63 (14 of them were major differences) paracrine factors by male and female amniotic stem cells. The debate on this inherent difference in paracrine factors between cells from male and female subjects has been prevalent in the literature. Another study revealed that hantavirus-infected female patients showed significantly higher plasma levels of interleukin-9, fibroblast growth factor 2, and granulocyte-macrophage colony-stimulating factor and lower levels of interleukin-8 and gamma interferon-induced protein 10 than male patients, demonstrating that a virus infection can induce sex-dependent differences in acute immune responses in humans [54]. Another study in 2013 conducted by Furman, et al. [55] reported elevated antibody responses to trivalent inactivated seasonal influenza vaccine and expression of inflammatory cytokines in the serum of females compared with males irrespective of age.

Sex-related differences in the secretion of insulin-like growth factor 1 and other factors in sex and age-matched liver samples from patients were documented in a study conducted by Adamek, et al. [56]. Women with chronic hepatitis C showed a significantly higher concentration of insulin-like growth factor 1 serum levels as compared to male patients of the same disease. This sex-dependent difference in paracrine secretion was reflected in adiponectin and leptin concentrations in epicardial

1.5 Sex Differences in Life Science Research

and subcutaneous athero-thrombosis in male and female patients. The researchers concluded from their results that the epicardial fat in women produced higher concentrations of the adipocytokines than that of men [57].

1.5.2 Cytoskeletal Differences among Cells

It has long been established that particle endocytosis is intimately involved with the cytoskeletal framework of the cell, prominently actin and myosin. Qualmann, Kessels, & Kelly [58] found that the actin cytoskeleton has several molecular links in receptor-mediated endocytosis pathways.

Whether or not there are differences in the structure and/or arrangement of the cytoskeleton between different cell types has not been taken up with great fervor in the literature as of now. Nevertheless, there have been some works that documented such differences as one of the additional observations of studies conducted on cellular differences in aspects that are either directly or indirectly related to the cell cytoskeleton (e.g. cellular endocytosis). In their experiments with mouse embryonic stem cells and fibroblasts and reprogrammed induced pluripotent stem cells, Boraas, Guidry, Pineda, & Ahsan [59] found that the latter showed a lesser developed cytoskeleton as compared to the embryonic fibroblasts. Furthermore, they found that the induced pluripotent and embryonic stem cell groups expressed cytoskeletal proteins in a heterogenous manner as most cells.

In yet another study, calcium-sensitive actin filament-bundling protein villin was found in greater abundance in vomeronasal organ dendritic microvilli but completely absent in the supporting cell microvilli (which had a higher abundance of actin filament cross-linking protein fimbrin) [60]. Studies conducted as far back as in the 1980s in astrocyte cells of certain amphibian species revealed that the said cell type of different nerves of the same animal differ drastically in their cytoskeletal and junctional components [61]. They also found profound differences in the cytoskeletal protein composition of the optic nerve and the spinal cord in fish, newts, and frogs as opposed to only minor polypeptide differences of the same nervous tissue types in mammals.

1.6 Other Uptake Determinants: Cancer Progression

One of the main objectives of this thesis is to establish a correlation between cytoskeletal differences that may exist between different cell types and variations in their respective endocytosis rates and mechanisms. This, being a topic that hasn't been explored so far in the literature, is sure to garner great interest among researchers and an equally high level of clinical significance.

1.6 Other Uptake Determinants: Cancer Progression

There is accumulating evidence in literature that cells from different stages of cancer (stage I to stage IV, primary tumor, or metastatic tumor) will have variations in their cytoskeletal elements and thus the mechanisms associated with the same. As mentioned before, endocytosis is one such mechanism. Bannasch et. al. [62] identified the presence of contractile proteins (like actin) in excess being an important prerequisite for malignant cells to spread metastatically. They also found that intermediate filament types like prekeratin, vimentin, and acidic glial fibrillar protein accumulate in various types of tumors. A number of other groups support this finding in their respective works [63, 64, 65, 66, 67, 68, 69]. Another group proved that cells that were less metastatic had large vinculin-containing focal adhesion points protruding from prominent stress fibers. Whereas cells with higher metastatic potential displayed unorganized actin bundles and vinculin [70].

Actin reorganization is integral for the morphology, migration, and invasion of cancer cells. The microtubule proteins, on the other hand, drive the process of cell migration induced in mesenchymal-turned primary cancer cells that have undergone EMT [71]. Epithelial to Mesenchymal Transition (EMT) is the process by which primary tumor cells lose epithelial characteristics and acquire migratory, mesenchymal phenotype. During EMT, the expression of many regulatory genes associated with actin is upregulated causing changes in actin organization and distribution [72]. At the secondary site, where the migratory mesenchymal tumors arrive after traveling through the blood stream, the cells undergo Mesenchymal to Epithelial Transition (MET) [73]. Hence, one may safely conjecture that the variation in cytoskeletal distribution of stage-varying tumor cells would in turn affect the particle endocytosis

1.6 Other Uptake Determinants: Cancer Progression

capacities depending on the source, type, and whether or not the tumor has metastasized from primary type via EMT.

Apart from the stage of cancer metastasis, research works state factors related to NP specifications (material, surface functionalization, size, charge, shape) [74] and the physiological environment at the nano-bio interface (protein corona, exposure time, pH, temperature, shear stress) that influence the overall nanoparticle uptake potential of a cell in question [75]. These factors will be probed in detail in the following chapters.

2

Background and Thesis Overview

The insufficient knowledge that exists in concepts of the nano-bio interface not only has a profound effect on the efficiency of nanomedicinal innovations but also has the potential to pose a big challenge for researchers and clinicians given the increasing importance of personalized medicine. Therefore, it is inevitable that we delve deeper into the uncovered realms of the cell-nanoparticle interface by taking into account all of the factors that might have a say in the cellular endocytosis of nanotherapeutics. This chapter describes the context of design of experiments and inferences derived at the end. The first few sections will discuss the main techniques and concepts followed in the materials and methodology portions of the thesis followed by descriptions of the project background, overview, and specific aims.

2.1 Description of Experimental Concepts

We have used a variety of techniques in the design of experiments, ranging from fluorescence-based methods for data acquisition like flow cytometry, confocal and super resolution microscopies, to mass spectrometric techniques (LC-MS/MS). Subsequent paragraphs will present a short introduction and the main principle behind each technique.

2.1 Description of Experimental Concepts

2.1.1 Flow Cytometry

Flow cytometry is a commonly used technique to obtain highly specific cell information. Apart from cell counting and sorting, flow cytometry may be used for the detection and/or measurement of protein expression, identifying cell cycle stage, post-translational modifications of proteins, cell viability and morphology, and even RNA. Fluorescent cells in suspension are passed through a detection system based on laser excitations and emissions. The fluidic, optic, and electronic systems in the machine work together to provide a robust cell analysis setup. A flow cytometer can reach upto speeds of thousands of particles per second, thus facilitating multiparameteric analysis of their chemical and physical properties.

In our experiments, we have used cell sorters and flow cytometers to retrieve pure cell populations from mixed cultures and analyze fluorescence signals from nanoparticle-treated cells respectively.

2.1.2 Confocal Microscopy

Confocal microscopy is one of the most common optical imaging techniques used in life science research owing to its features of obtaining high optical resolution and contrast, shallow field depth, optical sectioning, and ability to eliminate out-of-focus light. In a confocal microscope, the source laser scans one or more light beams across the sample, producing optical sections or images.

The microscope used for all the confocal imaging experiments in this thesis was a laser scanning microscope from Nikon. The laser scanning confocal microscope limits the sample focal plane to a very small volume by using pinhole apertures. Thus, successive optical sections along the z-axis of thick specimens can be obtained.

2.1 Description of Experimental Concepts

2.1.3 Stochastic Optical Reconstruction Microscopy (STORM)

Stochastic optical reconstruction microscopy is a type of super resolution microscopy technique that takes high resolution images without the drawback conferred from the diffraction limit (as is the case in conventional light microscopies). In STORM, a photoswitchable molecule emits photons consecutively when in activated state before “*switching off*” (dark state) or photobleaching (light deactivation) completely. This stochastic switching allows precise localization of the molecule, a random subset (optically resolvable fraction of molecules) of which, obtained from multiple snapshots of the specimen can be used to reconstruct a super resolution image.

2.1.4 Liquid Chromatography Tandem Mass Spectrometry (LC-MS/MS)

LC-MS/MS is a highly sensitive analytical chemistry technique combining liquid chromatography for physical separation and mass spectrometry for mass analysis of inorganic, organic or biochemical samples. In this system, the sample mixture (in this case proteins) is first separated by liquid chromatography followed by being ionized and characterized by two mass spectrometers in series according to the mass-to-charge ratio and relative abundances of each separated component. Data is obtained in the form of spectral counts which represents the number of MS/MS spectra identified as the ion abundance of the component species.

2.1.5 Transmission Electron Microscopy (TEM)

Transmission electron microscopes can image samples at a significantly higher resolution than conventional light microscopes. Hence, they can capture details to the order of a few angstroms in the sample. In a TEM, a beam of electrons is transmitted through an ultrathin section of the sample to form an image. Image formation occurs via the interaction of electrons with the specimen. This image is then magnified and focused onto an imaging device. Sample preparation to image biological samples with TEM consists of a complex series of steps including embedding in a resin and ultrathin sectioning

2.2 Factors Involved in Cell Nanoparticle Uptake

using a microtome.

2.1.6 Patient-derived Xenograft (PDX) Tumor Models

PDX tumor models are disease models of mice developed from implantation of tumors harvested from a patient. These models help mimic the in vivo tumor microenvironment that facilitates natural growth and monitoring of the patient. PDXs are extremely useful for cancer research purposes and/or for evaluating treatment strategies of the ailing individual. They are biologically stable and accurately imitate the histopathology, therapeutic response, gene expression, inflammation, and genetic mutations of the patient. For the purposes of our experiments, patient-derived tumors growing in mice were harvested and expanded in in vitro 2D cultures to perform uptake tests.

2.2 Factors Involved in Cell Nanoparticle Uptake

As seen from Chapter 1, there are a variety of factors determining the cell nanoparticle uptake ranging from patient-related factors to nanoparticle and environmental factors as listed below:

2.2.1 Patient and Disease-related Factors

1. **Patient Gender:** Being male or female is an important determinant that researchers often ignore in their study subjects. We have mentioned earlier that each cell has a sex and the same will have a profound effect on their ability to take up nanoparticles. We will explore this in depth in this thesis project.
2. **Patient Age:** Medicines are formulated and administered differently for infants, adults, and elderly people. Several studies stipulate that these differences have a root at the cellular level. We will investigate the possibility of the incidence of such differences.
3. **Disease Progression:** Cancer therapeutics targeted for early and late stage cancers are different due to varying patient responses. Disease progression can be interpreted also in terms of the

2.3 Thesis Overview

metastatic potential of the tumor. Primary tumor, migratory mesenchymal tumors (after EMT), and secondary tumors (after MET), will respond differently to nanoparticle interventions.

4. **Cancer Origin:** : In this project, we also investigate if the body part in which the cancer originates or migrates to has a say in the nanoparticle uptake capacities of the tumor cells.

Nanoparticle-based factors like the material of the nanoparticle, surface functionalization, size, charge, and shape have been shown to influence the uptake mechanisms and efficiency in several works cited in Chapter 1.

2.2.2 Environmental Factors

1. **Protein Corona:** We investigate the effect of protein corona of the nanoparticles used in the project and whether or not it is modified by the secretory proteins of the cells.
2. **Exposure Time:** We propose to do time-dependent experiments in future studies as the literature imparts great significance to the exposure time of the NPs in their biological fates.
3. **pH:** Since cells thrive at an ambient pH of 7 or slightly more basic than that, pH variation should influence NP uptake drastically.
4. **Temperature:** Like time, temperature is a factor that cannot be ignored and will be studied upon in future experiments.

2.3 Thesis Overview

We have seen that several groups have studied the interactions occurring at the nano-bio interface, sex differences in cell types, and the interdependence of the cytoskeleton and endocytosis pathways. However, there is still a dearth of any research on how the factors listed in section 2.2 affect events at the cell-nanoparticle interface. We evaluate this by dividing the thesis into two projects: the Cell Gender project and the Cancer Nanoparticle project. The cell gender project deals with studies in gender-

2.3 Thesis Overview

mismatched and age-matched primary salivary gland fibroblasts using quantum dot nanoparticles. We investigated the influence of patient (cell) gender, age, and protein corona on the uptake capacities of the cells. The cancer nanoparticle project takes into account the possible variations introduced by disease progression, cancer origin, and other factors. Experiments were conducted on primary cells expanded from patient-derived xenograft models developed from tumor resections of patients. Primary gastric tumor cells and lung tumors metastasized to the bone with polystyrene nanoparticles were used. Additionally, we propose to compare the NP uptake trends between pure tumors and corresponding stromal cells of the tumor cells.

2.3.1 Advantages of using Primary Cells over Cell Lines

Cell lines have long been the preferred complement to *in vivo* experiments. However, they may often differ genetically and phenotypically from their actual tissue of origin. Primary cells serve as a good alternative as they maintain several markers and protein expression profiles seen in their tissue of origin. Primary cell culture uses specially optimized media with less serum levels for optimal growth which is advantageous as excess serum is known to promote differentiation of the cells and/or foster expansion of contaminating cells like fibroblasts. Moreover, when researching topics that have a high clinical relevance, one must strive to be as close to *in vivo* conditions as possible and choosing primary cells over cell lines is one of the best ways of doing this.

2.3.2 Research Aims & Hypothesis

The aim of this thesis project is to evaluate the effects of the different factors involved in the cellular endocytosis of nanoparticles. We hypothesize that each factor listed in the Background section both individually and in combination with each other would cause changes in the cytoskeletal framework of the cells and related proteins, thus influencing their nanoparticle uptake mechanisms and abilities. This would translate to variations in targeting efficiencies by the same nanotherapeutic agent in each

2.3 Thesis Overview

case. In order to avoid these discrepancies, it is inevitable that we study these interactions in greater detail. This project can be considered as the stepping stone into this relatively novel field of research. Undoubtedly, we would need to conduct more detailed studies on a greater variety of cells to establish new facts in this area that can be incorporated into clinical uses.

2.3.2.1 Cell Gender Project

- To analyze nanoparticle uptake trends in salivary gland fibroblasts from opposite sex but age-matched patients
- To study the variations in actin distribution among the cells and find correlations with nanoparticle uptake trends
- To evaluate the difference in the protein coronas of the cells and thus elucidate distinctions in secreted paracrine factors

2.3.2.2 Cancer Nanoparticle Project

- To perform surface characterization studies on polystyrene nanoparticles
- To analyze nanoparticle uptake trends in various primary cancer cells
- To establish correlations in nanoparticle uptake, if any, among the pure tumors and pure stroma of a mixed tumor culture

3

Methodology

3.1 Cell Gender Project

In the cell gender project, we analyzed the influence of the gender and age of the patients along with environmental factors on the nanoparticle uptake responses of primary fibroblasts. The cells were isolated from salivary gland tissue and cultured to reach about 70% confluency. Quantum dot uptake studies were conducted via flow cytometric analysis and confocal imaging. Once the dominance of a gender group in NP uptake was established, we proceeded to analyze the causes of this difference using a super resolution microscopy technique called STORM, Transmission Electron Microscopy and proteomic studies.

Any fluorochrome (QDot and/or calcein-AM in this case) attached to the cells gets excited from the light beam in a flow cytometry chamber resulting in fluorescent emission data that can be collected for multiparametric analysis. Wide-field epifluorescence has disadvantages that can be alleviated using confocal microscopy. Similar to Total Internal Reflection Fluorescence (TIRF) Microscopy, it narrows the imaging volume without restricting to the glass-cell interface [76].

It is known that TEM provides the highest resolution and allows quantification of single NPs in

3.1 Cell Gender Project

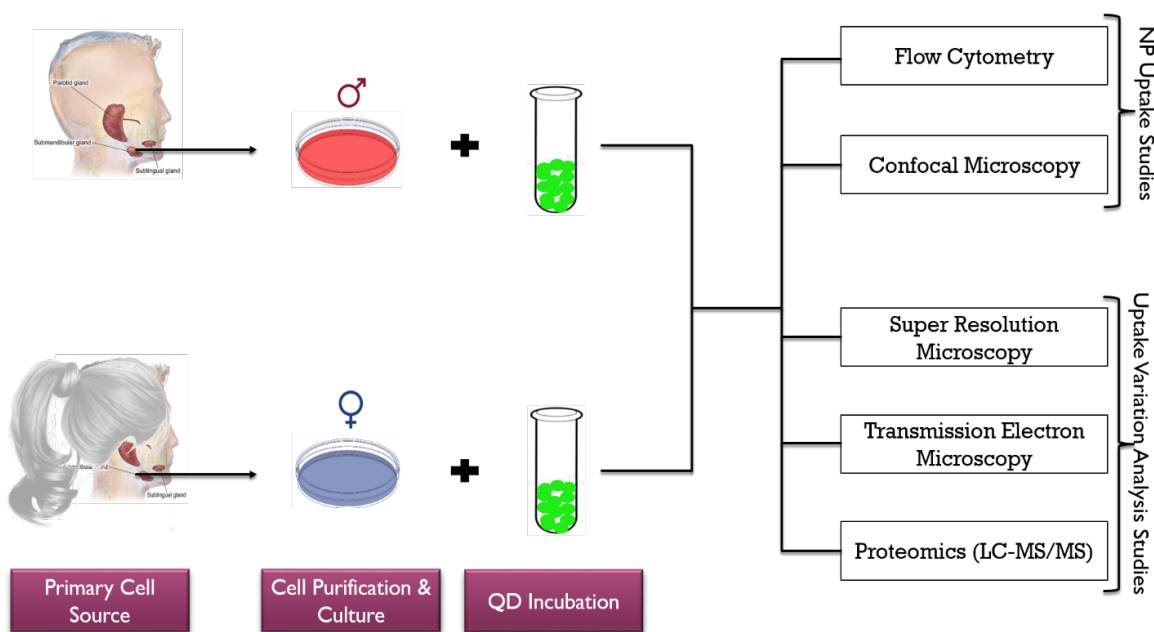


Figure 3.1: Overview of methodology followed for nanoparticle uptake studies and analysis in human salivary gland fibroblasts from 43-year-old male and 45-year-old female patients

sub-cellular structures [77]. Metal nanoparticles of size greater than 5 nm can be directly visualized intracellularly using TEM because of their high electron densities [78]. Zeta potential measurements are important because the cell membrane interacts differently with positive, negative and neutral charges on nanoparticles. It has generally been found that positively charged NPs exhibit an enhanced capacity of cellular internalization due to attractive electrostatic interaction between themselves and the negatively charged cell membrane, thus supporting uptake. Positively charged NP constructs, however, have been reported to have higher levels of cytotoxicity [79].

STORM imaging allows imaging and probing the interaction of nanoparticles with cellular components after internalization at the nanoscale resolution. Whereas super resolution imaging techniques like STED and SIM provide many interesting features (like better temporal resolution) for imaging nanomaterials within cells, STORM has the capability to provide information at the single molecule level along with unique image resolution [80].

3.1 Cell Gender Project

3.1.1 Materials

Submandibular salivary gland fibroblasts were obtained from patients aged 43, (female, Montreal General Hospital) and 48 (male, Collaborative Human Tissue Network (CHTN), The Ohio State University, Wexner Medical Center), courtesy Dr. Simon Tran's lab at the Faculty of Dentistry, McGill University. Qtracker 525 cell labeling kit (Q25041MP) was purchased from Invitrogen. For flow cytometry experiments, Calcein AM (C3100MP) was purchased from Thermo Fischer Scientific and FACS Canto II from BD Biosciences at Dr. James G Martin Lab, MUHC was used.

Plasma membrane of the cells were stained with *CellMaskTM* Deep Red Plasma membrane Stain (C10046) from Invitrogen for all imaging experiments. Confocal imaging was done in Ibidi 4 Well μ -Slides and imaged using a Nikon A1 Plus confocal microscope. Cells for TEM were cultured on Nunc Lab-Tek Chamber Slide eight-well Permanox slides and imaging was done using an FEI Tecnai 12 TEM. For Zeta Potential experiments, a NanoBrook ZetaPlus zeta potential analyzer from Brookhaven Instruments was used. F-actin labeling for STORM was done using Alexa Fluor 647 phalloidin from Invitrogen (A22287). Anti-Clathrin heavy chain antibody (ab21679) were used for clathrin heavy chain labeling. STORM imaging was done on a Nikon Eclipse Ti-U inverted optical microscope using an oil immersion objective (Nikon CFI Plan Apochromat λ 100 \times , NA 1.45).

3.1.2 Methods

3.1.2.1 Cell Isolation and Culture

Two submandibular salivary gland tissues were obtained from patients aged 43 (female, Montréal General Hospital) and 48 (male, Collaborative Human Tissue Network (CHTN), The Ohio State University, Wexner Medical Center). In both tissues, no pathological issues were reported. The isolation followed the general guidelines provided by the “*Establishment of Fibroblast Culture, Dissociated Fibroblast Culture*” from the Current Protocols in Cell Biology [81].

3.1 Cell Gender Project

Briefly, tissues were minced to 2-3 mm cubes using scalpels and incubated with collagenase I [CLS 1, Worthington, OH, USA], for 2h at 37 °C. Enzymatic activity was halted with media supplemented with fetal bovine serum. Tissues were placed in a 70 µm filter and washed with the supplemented RPMI. Centrifugation of the filtered liquid yielded a pellet of cells. Incubation with media in a T25 flask at 37 °C and 5% CO₂ led to cellular attachment and expansion to the desired cell numbers.

3.1.2.2 Flow Cytometry

A total of 50,000 male or female salivary gland fibroblasts were plated in a 24-well plate. For coculture experiments, female cells were incubated with Calcein-AM (in DMSO, ThermoFisher) for 30 min and washed three times using raw RPMI. A total each of 25,000 male and labeled female cells were cocultured in a 24-well plate. Cells were washed with PBS before QD treatment (Qtracker 525, Thermo Fisher Scientific). After 6 h of incubation with QDs, cells were harvested and washed three times with PBS. Cells were kept on ice until running through a FACSCanto II (BD). The data was then tested for significance by one-way analysis of variance (ANOVA).

3.1.2.3 Confocal Imaging

Salivary gland fibroblasts from 48- and 74-year-old male patients and 45- and 77-year-old female patients were cultured on Ibidi four-well µ-slides. Cultures were incubated with QDs for 6 h. They were then stained with CellMask Deep Red plasma membrane stain (Invitrogen) for 10 min at 37 °C. Following this, they were fixed in 3.7% glutaraldehyde and dehydrated using 0.1% sodium borohydride (5 min, 2 times). The fixed cells were then stained using DAPI and observed under a Nikon A1 Plus confocal microscope.

3.1.2.4 Confocal Image Analysis

The percentage of QD uptake by each cell was determined by quantifying the areas with QDs (green) in the images as compared to the whole cell (red) area using ImageJ software.

3.1 Cell Gender Project

3.1.2.5 Transmission Electron Microscopy (TEM)

The cells were cultured on Nunc Lab-Tek Chamber Slide eight-well Permanox slides. The cells were incubated with quantum dots or conjugated 10 nano gold particles for 6 h. Cells were fixed with 2.5% glutaraldehyde in a 0.1 M sodium cacodylate buffer (pH 7.4) and post-fixed in 1% osmium tetroxide. The samples were further fixed and stained with 1% tannic acid. After a final wash with the sodium cacodylate buffer, the specimens were dehydrated through a graded series of alcohol baths (30–100%) and then embedded in Epon resin. Ultrathin sections were cut using a ultramicrotome and transferred onto 200-mesh Cu TEM grids with a Formvar support film. The samples were imaged with an FEI Tecnai 12 TEM equipped with a Gatan CCD camera at an accelerating voltage of 120 kV.

3.1.2.6 Zeta Potential Analysis

Supernatants from male, female, and male–female coculture were collected after 24h of incubation. The quantum dots were incubated with plain cell media (control) and each supernatant for 1h. They were then centrifuged at 13000g to pellet the QDs. A 500 μ L amount of cold PBS was added to each tube to disperse the QDs. For zeta potential analysis a NanoBrook ZetaPlus zeta potential analyzer from Brookhaven was used.

3.1.2.7 Fluorescence Labeling for STORM Imaging

Salivary gland fibroblasts were cultured on #1.5 glass coverslips (12 mm diameter) as described above. Cells were initially fixed and extracted for 1 min with a solution of 0.3% (v/v) glutaraldehyde and 0.25% (v/v) Triton X-100 in cytoskeleton buffer and then post-fixed for 20 min in 2% (v/v) glutaraldehyde in CB. For fluorescent labeling of actin filaments, samples were incubated with AF647-conjugated phalloidin (Invitrogen A22287) at \sim 0.1 μ M. For clathrin imaging, the clathrin heavy chain was labeled with anti-clathrin heavy chain antibody (ab21679) and CF-568 conjugated secondary antibody against clathrin primary.

3.1 Cell Gender Project

3.1.2.8 STORM Imaging

STORM imaging was performed on a home-built setup based on a Nikon Eclipse Ti-U inverted optical microscope using an oil immersion objective (Nikon CFI Plan Apochromat λ 100 \times , NA 1.45). Imaging was done for actin filaments and clathrin protein according to the protocols [82, 83]. The cells were cultured on #1.5 glass coverslips. When they reach the desired confluency, the cells were treated with QDs for 6h and stained for actin filament and clathrin as explained earlier for the hAMSC cells. Lasers at 640 and 405 nm (Coherent) were coupled into an optical fiber after an acousto-optic tunable filter and then introduced into the sample through the back focal plane of the microscope. Using a translation stage, the laser beams were shifted toward the edge of the objective so that emerging light reached the sample at incidence angles slightly smaller than the critical angle of the glass-water interface (TIRF stage).

Continuous illumination of the 640 nm laser (\sim 80 mW for AF647) was used to excite fluorescence from labeled dye molecules and switch them into the dark state. Concurrent illumination of the 405 nm laser was used to reactivate the fluorophores to the emitting state. The power of the 405 nm laser (typical range 0-1 mW) was adjusted during image acquisition so that at any given instant only a small, optically resolvable fraction of the fluorophores in the sample were in the emitting state. The 640 nm laser power was increased from 1 mW to 15 mW over a period of about 15 min (for photobleaching), finally increasing the power to 80mW for raw data acquisition (blinking action of fluorophores). For clathrin imaging, image acquisition on the microscope was performed in the same way except that the 561 nm laser was used for excitation instead of the 640 nm one. The 640 nm laser was used to illuminate the plasma membrane dye for two-color imaging. Cell imaging was performed in an imaging buffer consisting of 50 mM Tris, pH 8, 10 mM NaCl, 168.8 units/mL glucose oxidase, 1404 units/mL catalase, 10% (w/v) glucose, and 20 mM MEA (cysteamine) [84]

3.1 Cell Gender Project

3.1.2.9 Liquid Chromatography Tandem Mass Spectrometry (LC-MS/MS)

Hard Corona Extraction:

Unsupplemented media was conditioned by male, female and coculture samples of salivary gland primary fibroblasts for at least 6 hours. The supernatants from each sample were collected and incubated with 4 ul of quantum dots for one hour. Control samples were incubated in raw unconditioned media. The samples were then centrifuged at 18,000 rcf for 5 minutes at 4 °C. The supernatants were discarded. The pellet was resuspended in 500 µl of cold PBS and centrifuged again (15,200 g, 5 minutes, 4 C). This washing step was repeated two more times to get rid of the proteins loosely bound to the NP surface (soft protein corona). The samples can be subsequently run through any proteomic analytic systems like mass spectrometry.

LC-MS/MS: 10 mL of the 12 ng/mL suspension of Trypsin Gold (Promega, V5280) was added to each sample of hard corona proteins and incubated overnight at 37 °C. 100 mL of acetonitrile was added to wash the peptides from the QDs and tube wall. The samples were spun for 30 seconds in a table-top centrifuge. The supernatant was transferred to a clean eppendorf tube and dried in a speed vac at medium heat. Subsequently, the dried peptides were re-suspended in 50 mL 0.1% formic acid in H_2O . It was then spun in an Eppendorf centrifuge at full speed. The top 40 mL was then carefully pipetted out into either a 96 well sample tray or into sample vials for LC-MS/MS run. The total spectral count for each peptide identified was noted and normalized via semi-quantitative assessment using the following formula:

X (Normalized Spectral Count for Protein 'k') =

$$\left[\frac{\left(\frac{SpC}{Mw} \right) k}{\sum_{i=1}^n \left(\frac{SpC}{Mw} \right) i} \right]$$

Where, SpC = spectral count and Mw = molecular weight in KDa for protein k

3.2 Cancer Nanoparticle Project

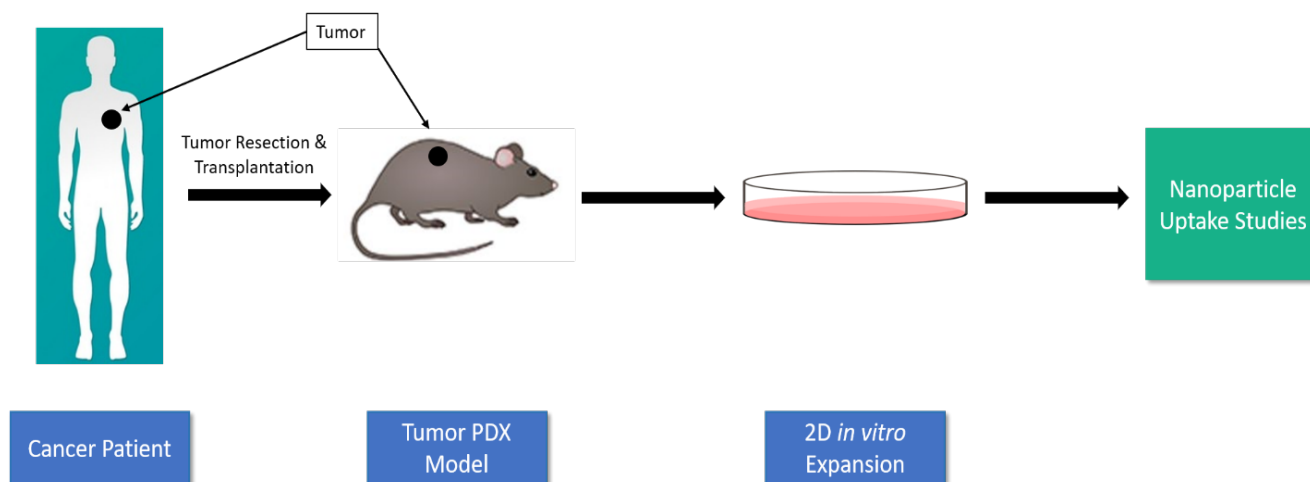


Figure 3.2: Overview of the nanoparticle cancer project.

3.2 Cancer Nanoparticle Project

The second part of the thesis focusses on examining the effect disease-dependent factors on NP uptake by tumor cells. Epithelial tumors were resected from various cancer patients in different stages of the disease and were implanted into immunodeficient mice. These tumors were then grown in culture with feeder layers derived from mouse fibroblasts. Culture conditions are controlled in such a way that murine fibroblasts are depleted, thus promoting tumor growth. The mixed tumor populations were then sorted into pure cancer cells and stromal cells using an epithelial cell marker. Following this, nanoparticle uptake studies were performed to quantify uptake capabilities of different cell populations.

As represented in 3.2, tumors from stomach were resected and transplanted into appropriate immunodeficient mouse models to establish a patient-derived xenograft (PDX) model. The tumors were extracted from the mice and expanded in vitro in 2D cultures following which, nanoparticle uptake studies were conducted.

3.2 Cancer Nanoparticle Project

3.2.1 Materials

Primary gastric cells, derived from PDXs were obtained from Morag Park Lab, Rosalind & Morris Goodman Cancer Centre, McGill University. Flash Red polystyrene nanoparticles (FSFR001) were purchased from Bangs Laboratories Ltd. For cell sorting experiments, epithelial cell marker BB515 Mouse Anti-Human CD326 (565398) (alternative name EpCAM) was purchased from BD Biosciences and FACS was done on FACS JAZZ from BD Biosciences. The viability dye used was the Zombie Green Fixable dye from BioLegend (423111). Flow cytometry experiments were done with BD Accuri C6 from BD Biosciences at the Department of Biological Sciences, Université du Québec à Montréal (UQAM).

Table 3.1: Cells in Cancer NP Project

Cell Name	Abbreviation	Disease Specification
GP2016136T	136T	Primary Gastric Tumor
GP2017181T	181T	Primary Gastric Tumor

Nanoparticle characterization involving dynamic light scattering (DLS) and zeta potential analysis was performed. The former was done using a Zetasizer Nano from Malvern Instruments Ltd. For zeta potential experiments, a NanoBrook ZetaPlus zeta potential analyzer from Brookhaven Instruments was used. Plasma membrane of the cells were stained with *CellMaskTM* Green Plasma membrane Stain (C37608) from Invitrogen for all imaging experiments. Confocal imaging was done in Ibidi 4 well μ -Slides and imaged using a Nikon A1 Plus confocal microscope.

3.2 Cancer Nanoparticle Project

3.2.2 Methods

3.2.2.1 Nanoparticle Characterization

100 mg/ml and 200 mg/ml solutions of polystyrene nanoparticles were made in dH_2O . They were allowed to sit at room temperature to stabilize. Following this, the samples were subjected to Dynamic Light Scattering (DLS). For zeta potential analysis, NanoBrook ZetaPlus zeta potential analyzer from Brookhaven Instruments was used.

3.2.2.2 Cell Sorting

The cells were trypsinized and resuspended in resuspension medium (1X DPBS, 5% FBS, 25mM HEPES). The cells were filtered with 70 μ m filter to avoid clumps. 5 μ L of EpCAM was added per 1 million cells and incubated on ice till flow run. The sorted cells were collected in recovery medium (FBS at least 90% + PenStrep 1% + media 9%).

3.2.2.3 Nanoparticle Uptake Studies

Cells were cultured to 70% confluency. After 24h, cells were washed one time with PBS followed by NP treatment. The cultures were labeled with 20 μ g/ml NP labeling solution and incubated at 37 °C for 6 hours.

3.2.2.4 Flow Cytometry

50,000 cells/well were plated in a 24-well plate and incubated at 37 °C for 24 hours. Following this, the cells were given 6h NP treatment. After NP incubation, the cells were washed with PBS and trypsinized. They were then collected and spun down and the supernatant was discarded. The cell pellet was resuspended in 1 ml PBS and spun down again. The cell pellets were resuspended in 100 μ l of diluted zombie green viability dye (BioLegends, 423111) and incubated for 10 minutes in the dark

3.2 Cancer Nanoparticle Project

at room temperature. The cells were then run through the BD Accuri C6 flow cytometer.

3.2.2.5 Confocal Microscopy

Cells were cultured on Ibidi four-well μ -slides. Cultures were incubated with NPs for 6 hours. They were then stained with CellMask Green plasma membrane stain for 10 min at 37 °C. Following this, they were fixed in 4% paraformaldehyde (in PBS) for 20 minutes in the freezer. The fixed cells were then stained using DAPI and imaged under a Nikon A1 Plus confocal microscope.

4

Nanoparticle Uptake Studies

4.1 Cell Gender Project

Nanoparticle uptake studies using a flow cytometer and confocal microscope were conducted after incubating cells with QDs for 6 hours. The data obtained is listed below:

4.1.1 Flow Cytometry

Flow cytometry readings were taken for single population and co-population cultures after QD treatment. The flow cytometry plots in [4.1](#) clearly show that male salivary gland fibroblasts take up more QDs than female cells. The percentage of positive male cells is roughly 2.5 times more than the female positives. The difference between the two cell types in MFI readings is, however, less drastic.

Co-culture experiments were done by labeling the female cells with Calcein-AM which is a plasma membrane-permeable live-cell labeling dye. Apoptotic and dead cells, however, do not retain the stain. In this way, we can distinguish between the male and female cell populations. [4.2](#) shows a contrasting result in terms of the percentage of cells and mean fluorescence intensity. Positive cells in the male category was approximately seven times than that of the female category. The corresponding MFI data

4.1 Cell Gender Project

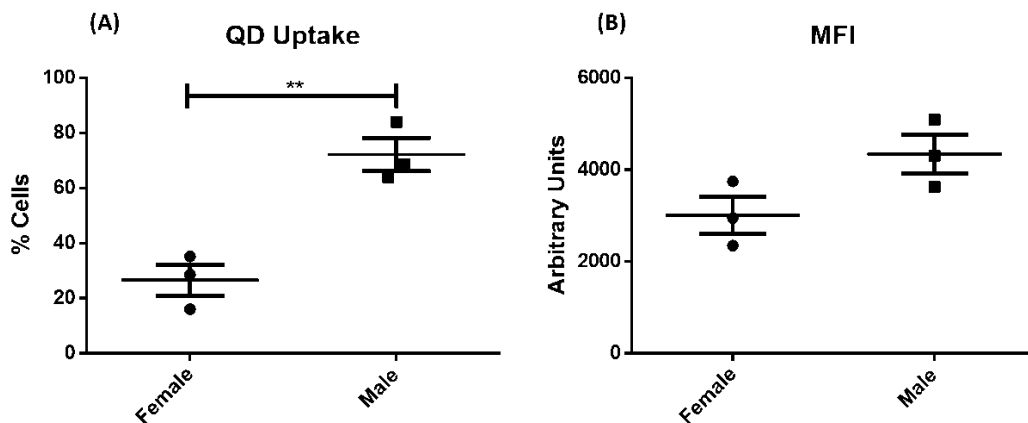


Figure 4.1: Flow cytometry plots showing quantum dot uptake by single-population male and female salivary gland fibroblasts. (A) depicts the percent cell count for each group for three repeats denoted by solid circles (females) and squares (males). The same data is shown in the form of mean fluorescence intensity (MFI) in (B). Two asterisks (**) indicates a p-value lesser than 0.01

reflects the male dominance in the co-population.

In 4.3, we see both MFI and positive cell counts together for the co-culture experiment. The solid horizontal lines across the histograms clearly demarcates the control population from the positive reading for male (orange) and female (blue) populations. QD+ 1.97 indicates that 1.97% of the total cells took up QDs while 98% did not (QD - 98.0).

4.1.2 Confocal Imaging

Confocal microscopy allows multi-color imaging of QD-treated male and female cells as seen in Figure 4.4.

All panels in Fig. 4.4 represent images of two sets of patients with matched ages belonging to opposite sexes. In some cells, for example 4.4A, there is comparatively more QD accumulation (in green) than other samples(4.4).

4.1 Cell Gender Project

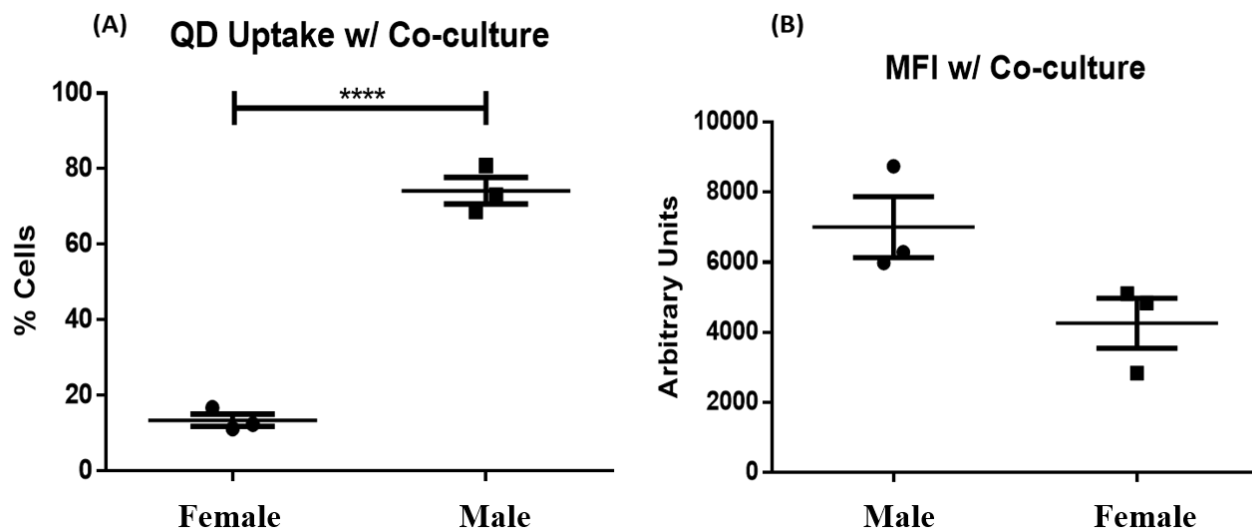


Figure 4.2: Flow cytometry plots showing quantum dot uptake by co-culture of male and female salivary gland fibroblasts. (A) depicts the percent cell count for each group for three repeats denoted by solid circles (females) and squares (males). The same data is shown in the form of mean fluorescence intensity in (B). Four asterisks in (A) denote a high statistical significance of p -value < 0.0001 .

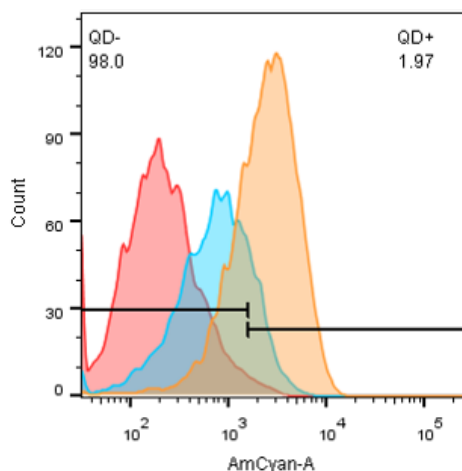


Figure 4.3: Quantum dot uptake histograms for the co-culture experiment showing absolute uptake cell count in red for unlabeled population, female population in blue and male population in orange.

4.1 Cell Gender Project

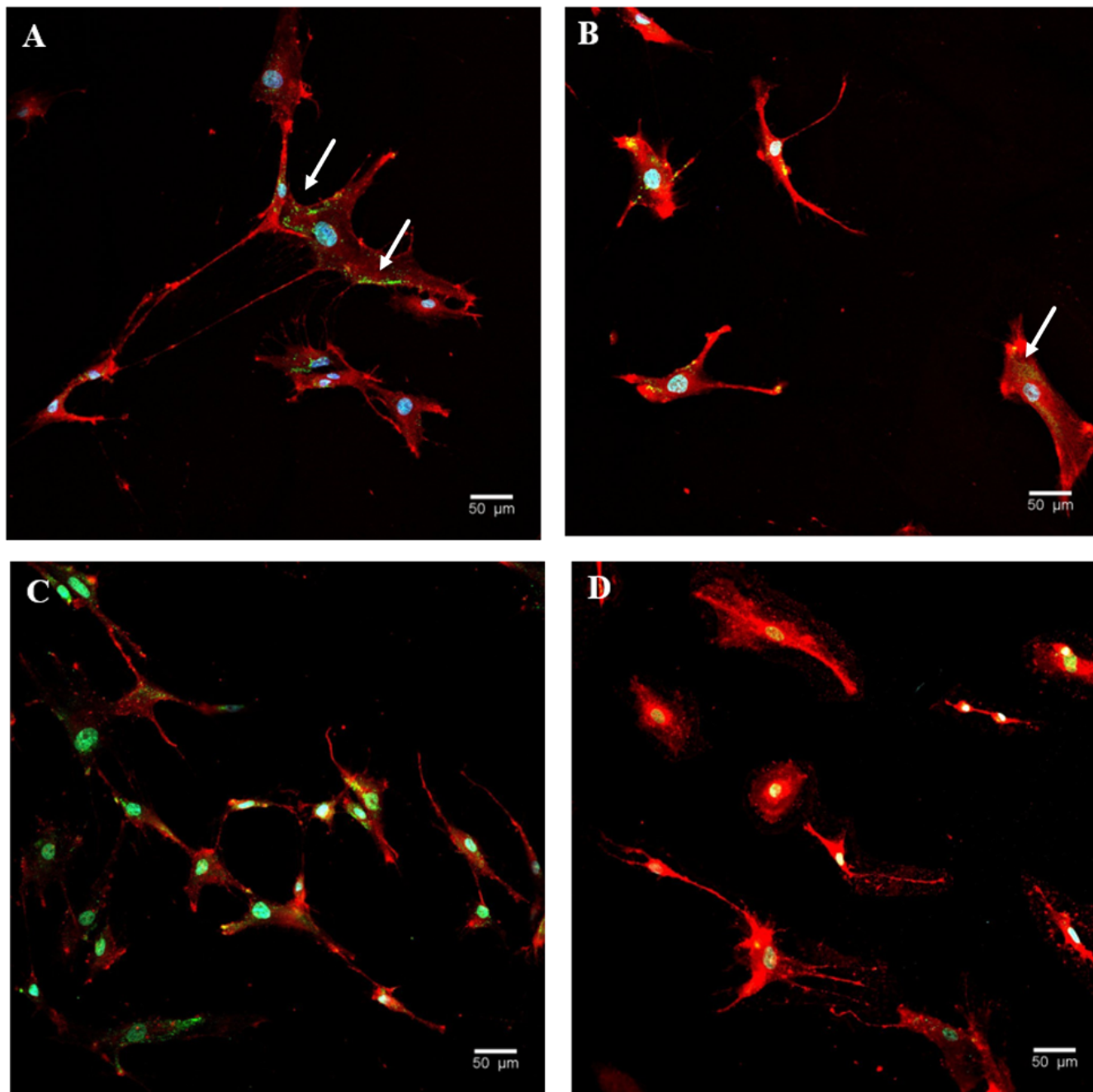


Figure 4.4: Confocal images of QD treated salivary gland fibroblasts from a 48 year old male (A) versus a 45 year old female patient (B) and a 74 year old male (C) versus a 77 year old female patient (D). (Red - Plasma Membrane, green - QDs, blue - DAPI). White arrows show green areas where QDs have accumulated. Scale bar is $50 * 10^{-6}$ m.

4.2 Cancer Nanoparticle Project

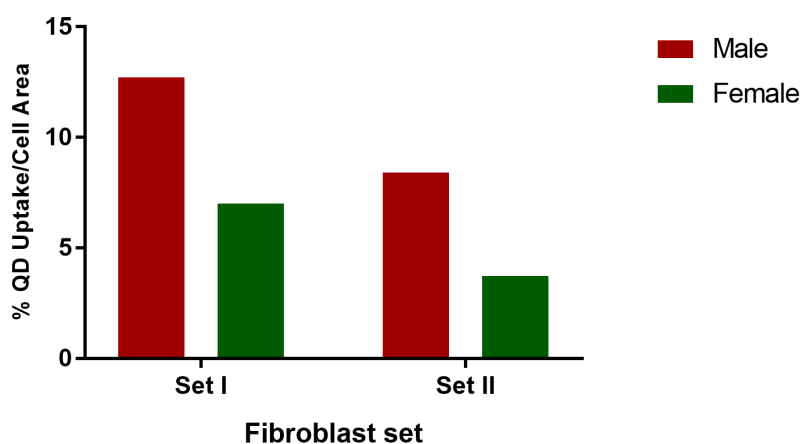


Figure 4.5: Percentage of QD uptake from each gender group quantified using confocal images and ImageJ. Male cells from both age-matched groups (A - 48 year old male and 45 year old female; B - 77 year old male and 74 year old female) internalize more QDs.

4.1.2.1 Confocal Image Analysis

Image analysis was performed using ImageJ software by quantifying the relative QD accumulation (green areas) with respect to the entire cell area (red area). We see that our results from confocal imaging and subsequent analysis corroborates the data from the flow cytometry experiment, re-affirming that male salivary gland fibroblasts take up more quantum dots than their female counterparts. This holds true for two fibroblast sets from two different age groups.

4.2 Cancer Nanoparticle Project

As mentioned before, the cancer nanoparticle project will focus on the analysis of changes in NP endocytosis due to variations in disease (cancer) states of the patient.

4.2.1 Nanoparticle Characterization

Characterization of flash red polystyrene nanoparticles gave an average hydrodynamic diameter of 67 nm and a negative zeta potential of 34.08 ± 1.87 mV. These values are in the expected range for the

4.2 Cancer Nanoparticle Project

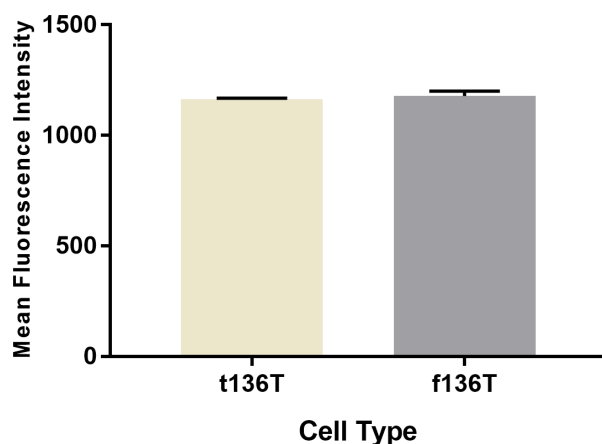


Figure 4.6: Mean Fluorescence Intensity of NP - treated samples measured via flow cytometry.

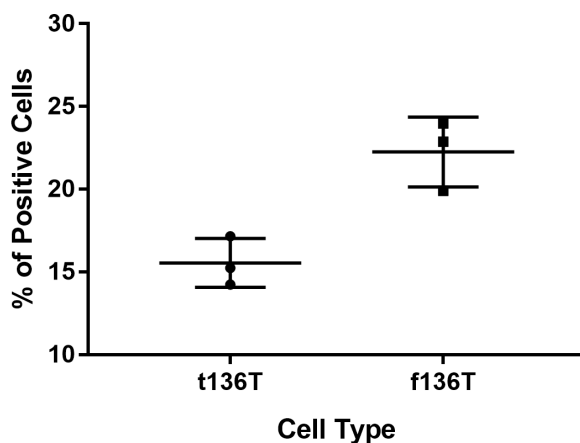


Figure 4.7: Percentage of cells for each type that endocytosed nanoparticles.

commercial nanoparticles according to the company datasheet values.

4.2.2 Flow Cytometry

Flow cytometric analysis after 6 hours of incubation shows that uptake capabilities of both the tumor (t136T) and stromal (f136T) population of the 136T cells are almost the same 4.6. Figure 4.7 shows the distribution of positive cells across the various test samples. The stromal population has a slightly higher number of positive cells than their tumor counterparts.

4.2 Cancer Nanoparticle Project

4.2.3 Confocal Imaging

Confocal images of the 136T tumors show accumulation of polystyrene nanoparticles in red (panels A2, B2, C2). Panel C indicates a collection of cells that are closely interacting with each other. Particle accumulation is seen only in few cells on one side while the others are almost devoid of red fluorescence from the nanoparticles.

Figure 4.9 shows the confocal images of nanoparticle-treated 181T tumors. All panels on the right side of the figure show nanoparticle uptake by the cells in red.

4.2 Cancer Nanoparticle Project

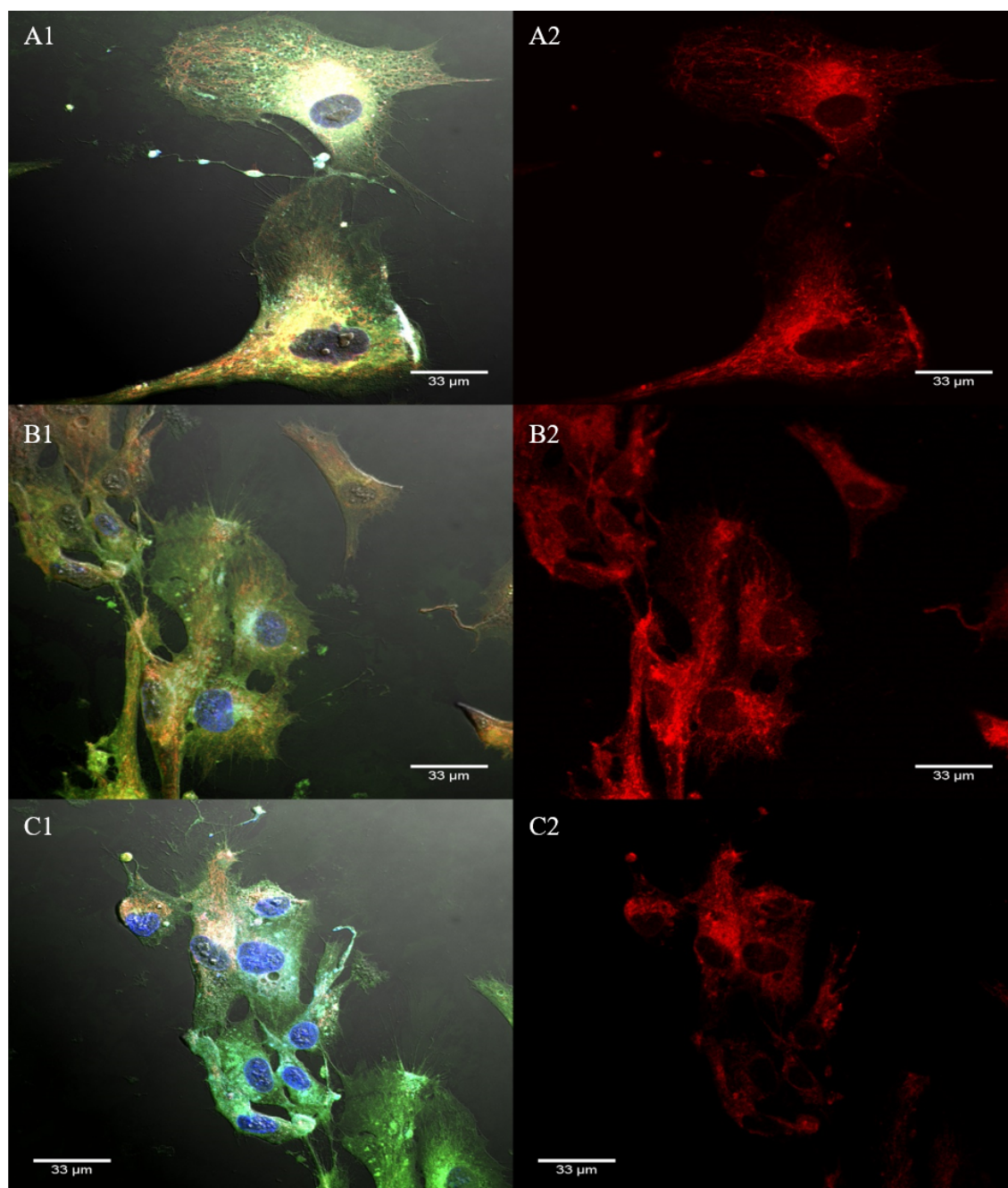


Figure 4.8: : Confocal images of nanoparticle - treated cells extracted from 136T tumors. The cell membrane is labeled in green, nucleus with DAPI (blue), and nanoparticles in red. Panels A2, B2, and C2 show nanoparticle accumulation in the cells. Scale bar is $33 * 10^{-6}m$

4.2 Cancer Nanoparticle Project

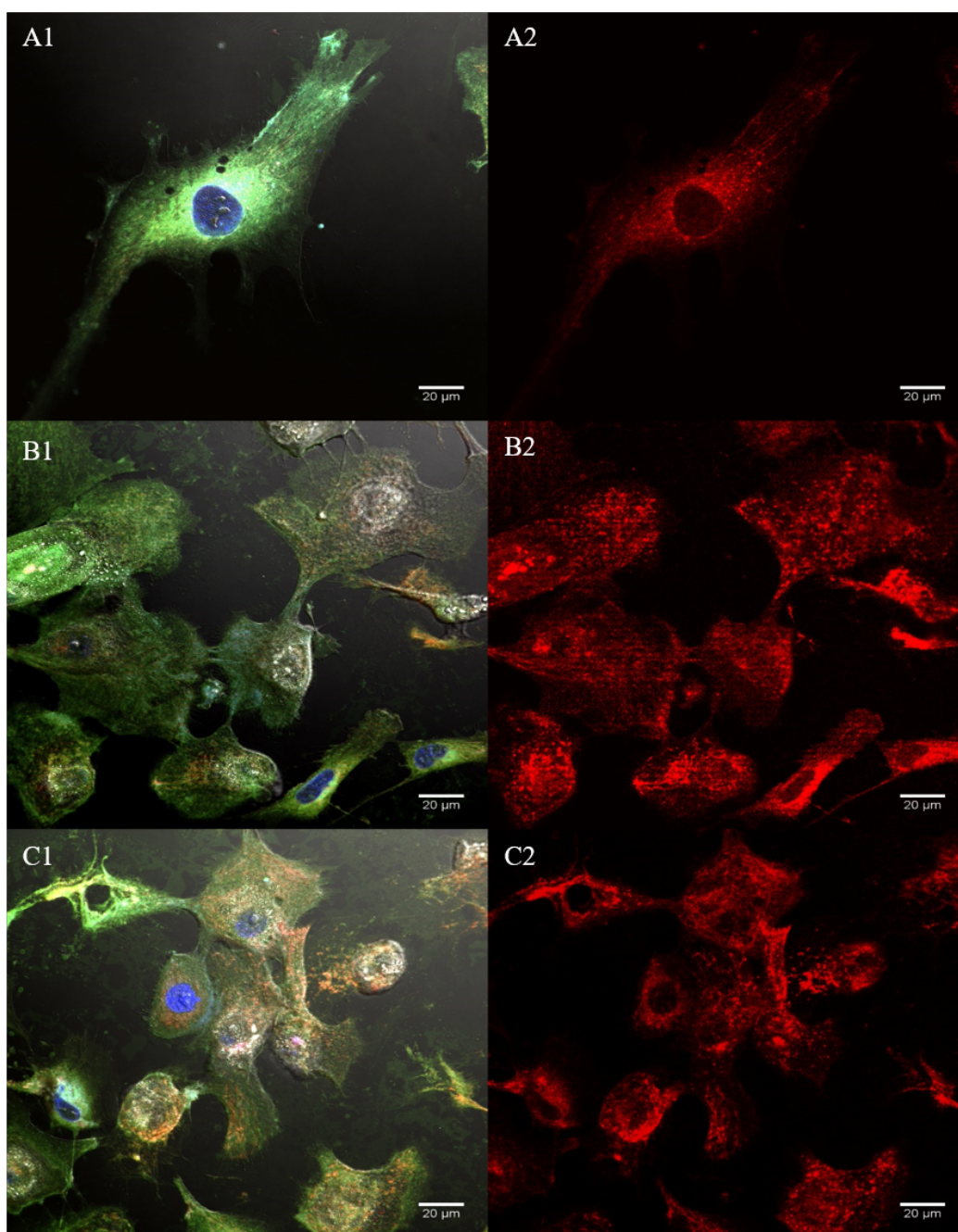


Figure 4.9: Confocal images of nanoparticle - treated cells extracted from 181T tumors. The cell membrane is labeled in green, nucleus with DAPI (blue), and nanoparticles in red. Panels A2, B2, and C2 show nanoparticle accumulation in the cells. Scale bar is $20 * 10^{-6}m$

5

Uptake Variation Analysis Studies

This chapter details the studies conducted to examine the reason behind higher NP uptake by one cell type over the other. Microscopy techniques (STORM and TEM) were used to image the actin and clathrin heavy chain coat protein distribution in cells. Proteomic studies on the hard corona of the QDs showed the influence of cell secreted proteins on the biological fate of the QDs.

Having established that male salivary gland fibroblasts internalize a greater amount of quantum dots than female fibroblasts, we then proceeded to further analyze why this difference occurs. As mentioned before, we hypothesized that the difference in NP uptake in salivary gland fibroblasts was caused primarily due to (but not limited to) (I) sex-dependent cytoskeletal differences, and (II) variations in secreted paracrine factors between male and female cells. We proceeded to analyze the former using super resolution microscopy and TEM and the latter by proteomic studies.

5.1 Cytoskeletal Analysis

Control and NP-treated cell samples were imaged with STORM and TEM and the results were compared to detect any definite patterns of actin and/or clathrin distribution.

5.1 Cytoskeletal Analysis

5.1.1 Super-Resolution Microscopy (STORM)

Stochastic Optical Reconstruction Microscopy technique was employed to analyze the differences in actin organization in male and female cells after labeling with an F-actin specific photoswitchable dye. By staining the plasma membrane of the cells, we could perform two-color imaging. To probe the abundance and distribution of clathrin heavy chain before and after treating the cells with QDs, we used antibodies specific to clathrin conjugated to a photoswitchable probe.

5.1.1.1 Actin Imaging

Two-dimensional STORM images of somatic primary fibroblasts demonstrated that the female (Figure 5.1 C & D) and male (Figure 5.1 A & B) cells have different organization, distribution, and morphology of actin filaments/bundles and, thus, show different outcomes in terms of QD uptake. In particular, fluorescence images of male cells stained for actin show a greater proportion of actin in thick bundles, which are likely stress fibers, around the periphery of the cells with little or no prominent filaments in the rest of the cell area. A considerable proportion of the actin in female cells was diffusely organized throughout the cell body. Female cells did not show any significant accumulation of stress fibres on the periphery.

5.1.1.2 Clathrin Imaging

We probed the localization of the clathrin heavy chain to the cell surface of both female and male salivary gland fibroblasts before and after incubation with the QDs (see Figure 5.2). Super-resolution images for the control (Fig. 5.2 a and d) and treated (Fig. 5.2 b, c, e, f) samples reveal that the primary female and male salivary gland fibroblast cells (Fig. 5.2 a - c) show evenly distributed clathrin staining prior to QD exposure. Following incubation with the QDs, the clathrin heavy chain remains more evenly distributed throughout the female cells, while male cells have increased localization of clathrin heavy chains to large punctae (Fig. 5.2 d - f).

5.1 Cytoskeletal Analysis

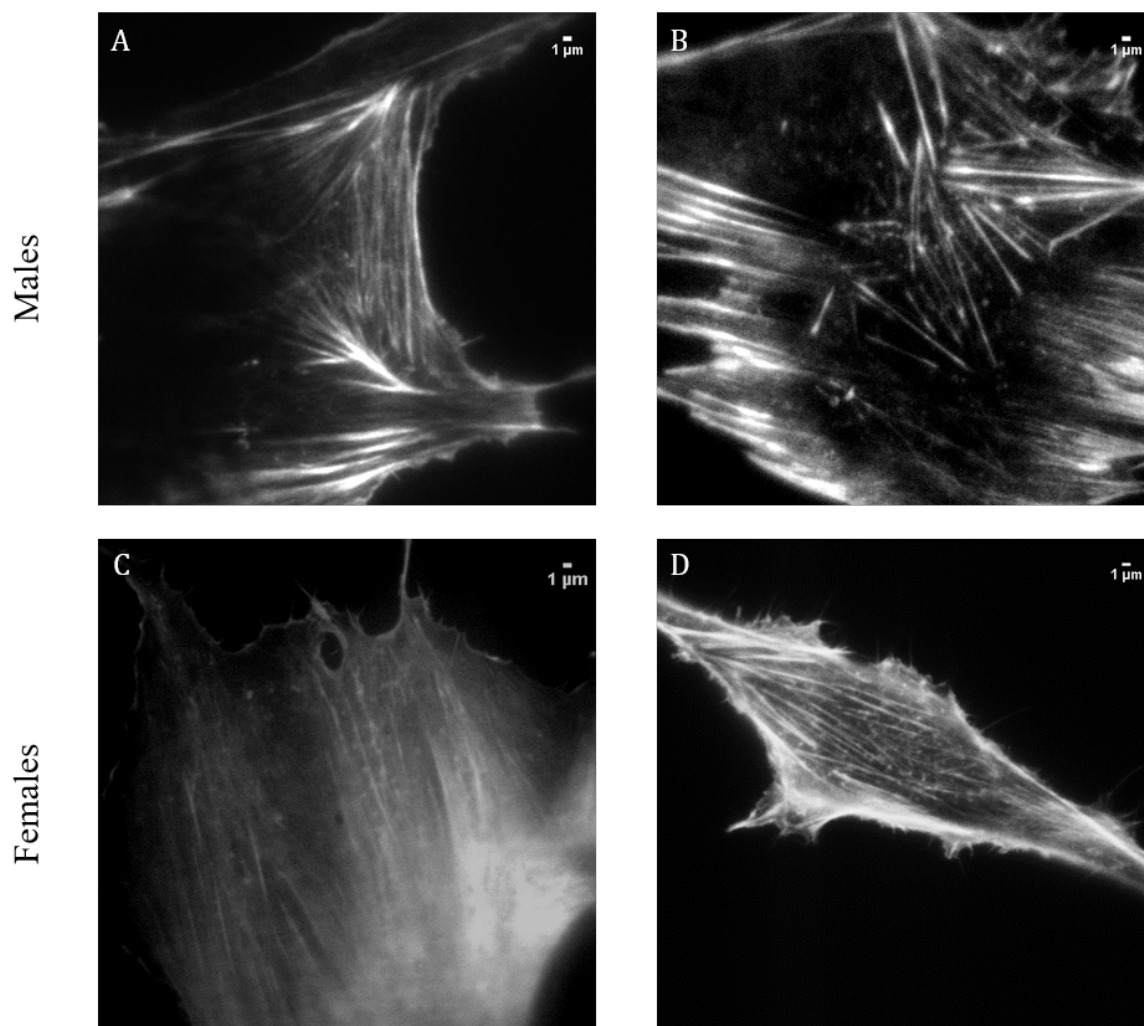


Figure 5.1: Super resolution images showing differences between organization, distribution and morphology of actin filaments or bundles in salivary gland primary fibroblasts extracted from the male (A, B) versus female (C, D) patients. Scale bar is $1 * 10^{-6}m$

5.1 Cytoskeletal Analysis

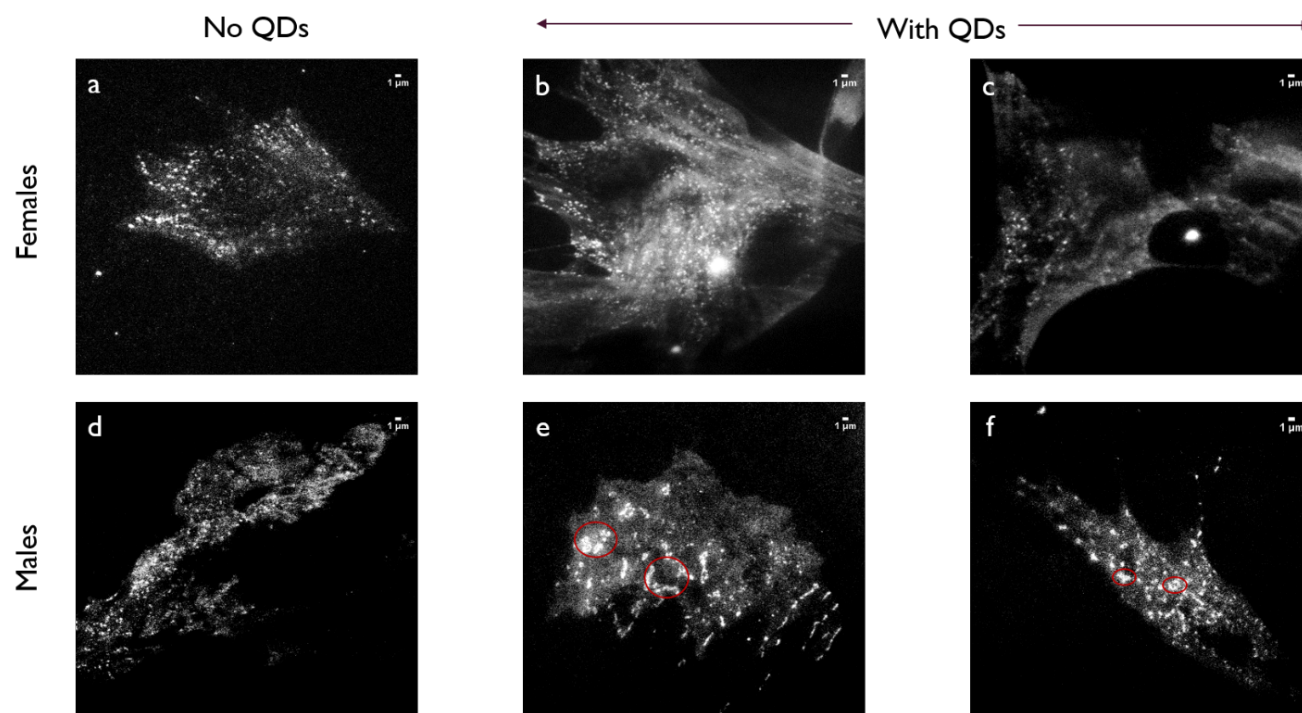


Figure 5.2: Super resolution images showing the arrangement of clathrin heavy chains in both female (a to c) and male (d to f) cells before and after incubations with QDs. Red circles in male treated cells indicate localization of clathrin to coated pits. Scale bar is $1 * 10^{-6}m$

5.1 Cytoskeletal Analysis

The increased concentration of clathrin heavy chains found on the male somatic fibroblasts, which have fewer actin filaments, correlated with greater and more rapid QD uptake. Super-resolution images also revealed a distinct linear arrangement of clathrin pits.

5.1.2 Transmission Electron Microscopy (TEM)

Given the high image resolving capabilities of a TEM, we employed the technique to see if the observations validated those in super resolution imaging. TEM micrographs confirmed that female cells exhibited a dense network of individual actin filaments throughout the cell (Figure 5.3 A and B). The bundle of filaments seen near the top of the image (Figure 5.3 A) is most likely actin stress fibers similar to those seen in the fluorescence image (Figure 5.1 A, B). In TEM, we cannot rule out that this bundle may also contain intermediate filaments and microtubules. The TEM images (Figure 5.3 C and D) of the male cells show a much less dense network of actin filaments, as is also evident by the lack of diffuse fluorescent signal in the light microscopy images (Figure 5.1 A and B) of the male cells. Based on the TEM analyses, it seems that microtubules are more abundant in male cells.

In an attempt to visualize the QDs within the fibroblast cells, we prepared parallel samples for TEM analyses. Considering the dimensions and the contrast of cadmium sulfide QDs are very similar to ribosomes and other protein complexes in the cell, it was not possible to detect them with confidence. Alternatively, we incubated the cells with conjugated 10 nm gold NPs [78]. Although distinction of gold NPs from the background was also challenging, it was possible to show their presence (Figure 5.4). Owing to the high density of gold NPs, they diffract under the electron beam, resulting in the appearance of a white spot under over-focused conditions. The results suggest, however, that the internalization of NPs is non-specific.

While clathrin-coated and other endosomal vesicles could be visualized in large numbers (Figure 5.5), only a few of the gold NPs could be visualized in endosomes or lysosomes (Figure 5.4 B); the gold NPs were found exclusively in non-coated vesicles. However, isolated or aggregated gold par-

5.1 Cytoskeletal Analysis

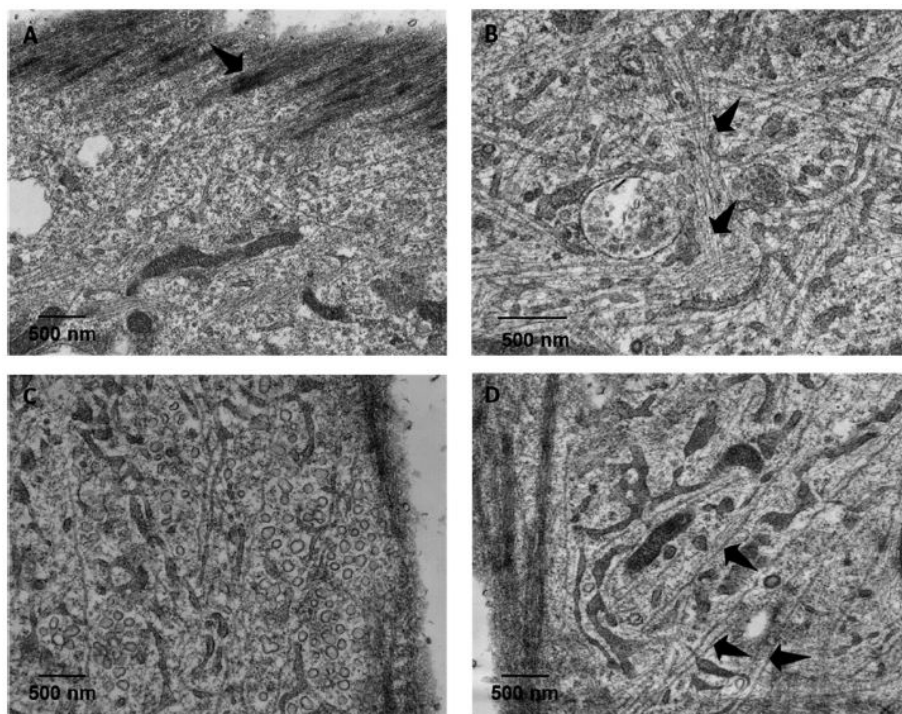


Figure 5.3: TEM images of salivary gland female (A, B) and male (C, D) control fibroblast cells. The female cells exhibit a dense network of filaments throughout the cells and a bundle of stress fibers close to the cell surface (arrow at the top of A). The male cells have much fewer filaments within the cells. Microtubules are more abundant in the male cells compared to the female.

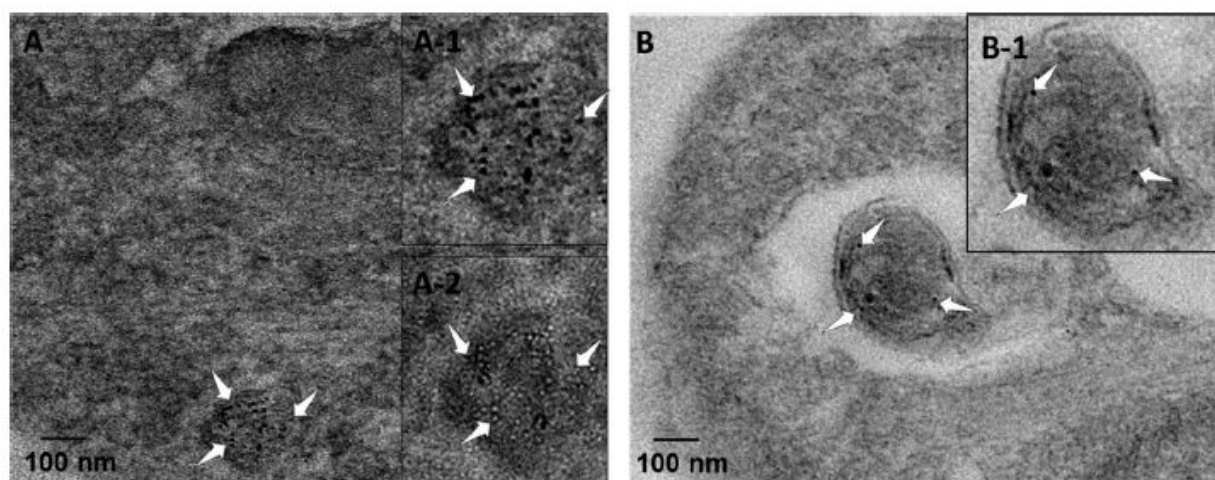


Figure 5.4: TEM images showing 10 nm gold NPs. Gold NPs can be seen within the cytoplasm of a salivary gland male fibroblast cell (A). White arrows point to gold particles. A1 is a close up of the gold aggregates, and A2 shows the same particle under overfocused conditions. (B) Inclusion of gold NPs in the lysosome. B1 is a close up showing an individual gold particle.

5.2 Zeta Potential & Proteomic Analysis of QD Corona

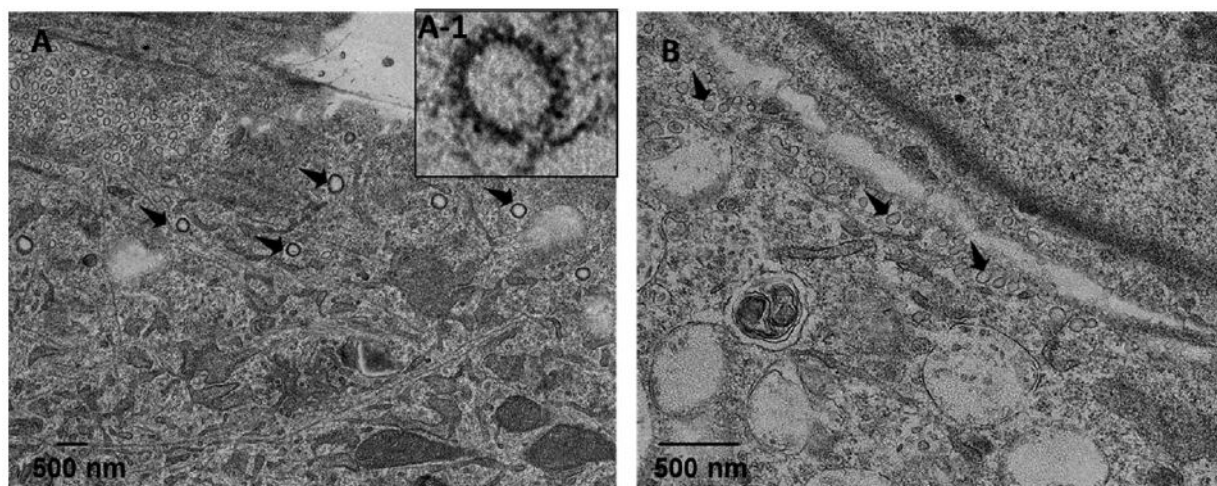


Figure 5.5: TEM images showing the presence of clathrin coated (A) and caveolae (B) vesicles in a salivary gland male fibroblast cell. There are no gold NPs present inside any of these vesicles. Some of the clathrin coated vesicles contain some gold particles on the outer surface (inset A1 in A).

ticles were visualized within the cytosol (Figure 5.4 A). Some of these gold NPs were associated with clathrin on the outer surface of clathrin-coated vesicles (insert A-1 in Figure 5.5 A), consistent with the light microscopic images, but on the cytoplasmic side of clathrin-coated vesicles or pits. The TEM micrographs in Figure 5.6 reveal alignment of coated vesicles along actin filament bundles, resembling clathrin-coated vesicles as was seen in Figure 5.2.

5.2 Zeta Potential & Proteomic Analysis of QD Corona

In the instance that a nanoparticle acquires a protein corona, two major phenomena gain relevance. Surface adsorption of proteins can change the surface charge of the nanoparticle, thus affecting several variables of its cellular internalization. Surface charge before and after exposure to cell-secreted factors was measured using a zeta potential analyzer. Additionally, we analyzed the hard corona of QDs incubated in cell supernatant of male and female cells using Liquid Chromatography Tandem Mass Spectrometry (LC-MS/MS) to determine if the sex distinction affected the composition of the corona.

5.2 Zeta Potential & Proteomic Analysis of QD Corona

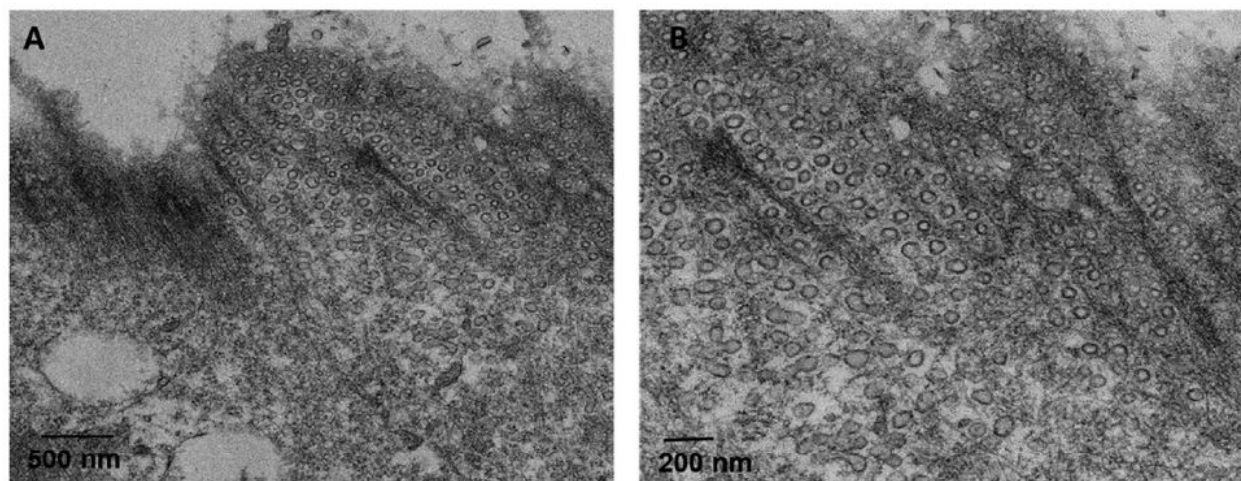


Figure 5.6: TEM images of the salivary gland female fibroblast cell revealing the linear alignment of coated vesicles along stress fibers in agreement with the super-resolution images

Table 5.1: Table showing zeta potential values of QDs both before and after conditioning with cell supernatants from male, female and co culture samples

Zeta Potential Measurements		
1	QD Controls	-23 ± 7 mV
2	QD + Male Cell Supernatant	-14 ± 5 mV
3	QD + Female Cell Supernatant	-14 ± 5 mV
4	QD + Male/Female Co-culture Supernatant	-5 ± 3 mV

5.2.1 Zeta Potential Analysis

The zeta potentials of surface-modified QDs were -14 ± 5 and -13 ± 4 mV, respectively, after incubation in male and female salivary gland cell supernatants. The zeta potential of QDs incubated in male - female coculture supernatant, however, dropped to -5 ± 3 mV (Table 5.1).

5.2.2 Liquid Chromatography Tandem Mass Spectrometry (LC-MS/MS)

In order to probe significant differences in the protein corona signatures of male, female, and co-culture cell supernatant-incubated QDs, we performed proteomic studies. Through repeated steps of centrifugation and washing the hard corona of QDs incubated in cell supernatants was extracted, purified and prepared suitably for proteomic analysis via LC-MS/MS.

5.2 Zeta Potential & Proteomic Analysis of QD Corona

Figure 5.7 shows a clear difference in the distribution and abundance of secreted paracrine factors between the male, female and co-culture samples. Some of the proteins are completely absent from the corona of certain samples (like proteins from mucin-16 to annexin A2 are absent in the male NP corona, Figure 5.7) while others are common in two or all three groups. We also observe differences in protein abundance with kallistatin being the most abundant in all three groups. Hemicentin protein, on the other hand, has the least spectral count (0.003 and 0.004 in female and co-culture coronas). Another noteworthy observation is that proteins absent in male and/or female corona appears in the co-culture corona.

5.2 Zeta Potential & Proteomic Analysis of QD Corona

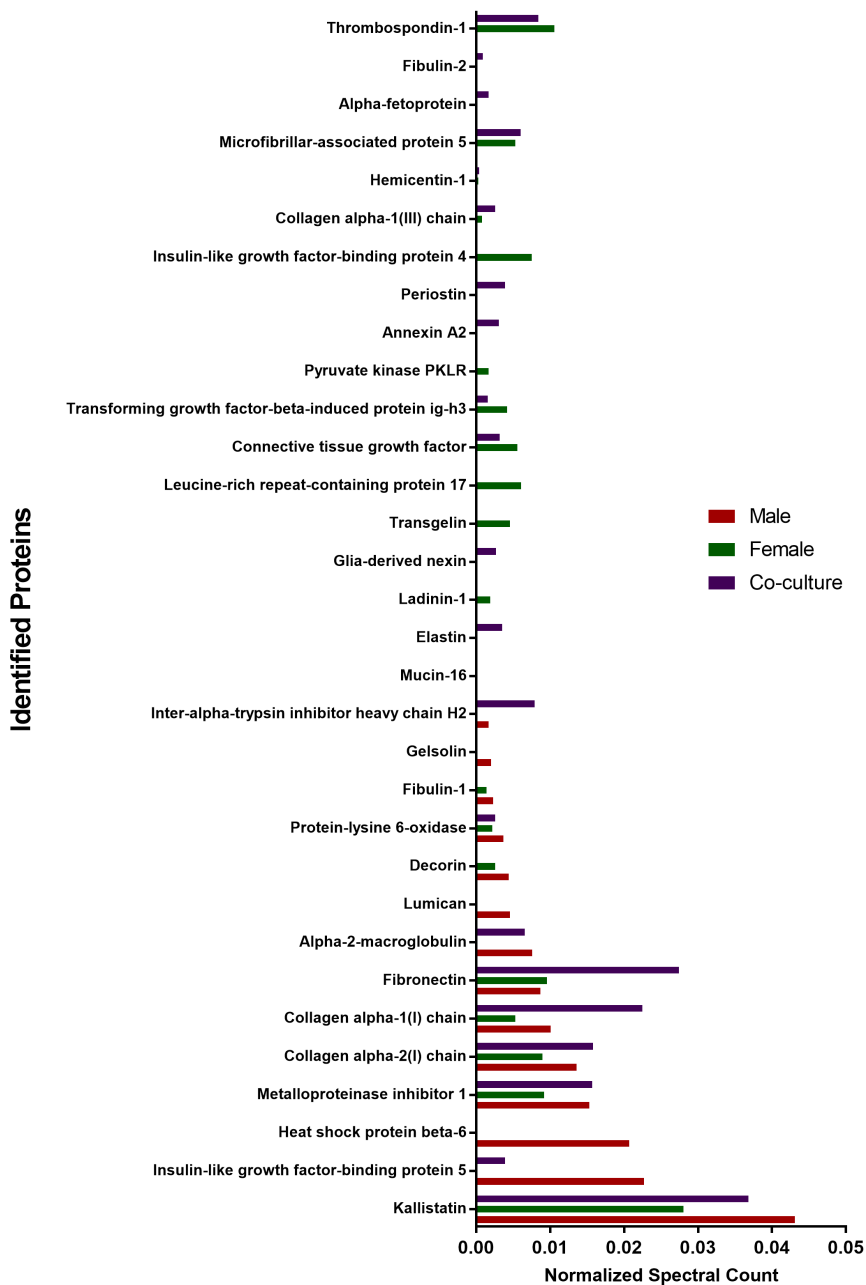


Figure 5.7: Graph showing normalized spectral counts of secreted proteins identified in the male, female and co culture protein coronas.

6

Discussions and Conclusion

6.1 Discussions

6.1.1 Flow Cytometry

Fluorescently labeled quantum dot signal in cells can be quantified using the flow cytometer. From 4.1, we see that male salivary gland fibroblasts endocytose a higher quantity of QDs as compared to the females. The single sex cell population experiments confirm that the difference in QD uptake is caused by sex-based structural differences in the cytoskeleton of the cells and/or secreted paracrine factors. This is further verified by co-culture experiments using prelabeled female cells cultured with an equivalent number of unlabeled male cells prior to QD treatment. Co-culture figures (4.2, 4.3) depict how the male population still shows higher QD accumulation despite the presence of female cells. The fluorescence is in fact slightly more than the fluorescence from the single population study (see panel B's in 4.1 and 4.2). Although equal numbers of cells from each type were seeded initially, MFI data from 4.2B shows that either male cells take up more quantum dots per cell or they proliferate at a higher rate than the females thus dominating the culture area. The latter proposition doesn't seem highly likely as the cultures weren't incubated for more than 24 hours for one cell type to overpopulate the culture. In

6.1 Discussions

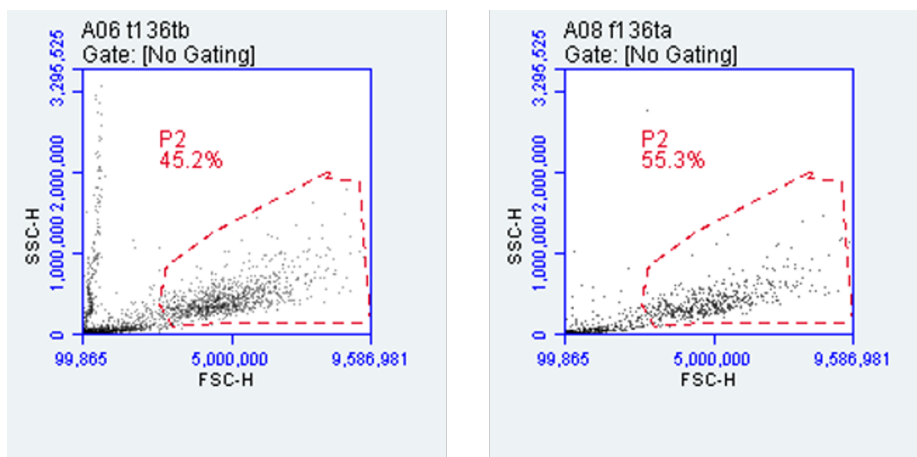


Figure 6.1: Forward and side scatter characteristics of a typical flow run of NP-treated t136T and f136T gastric cells.

the coculture experiments the quantity of actin filaments, as well as their organization, could influence QD uptake, as the actin-rich female cells do not take up as great a concentration of QDs as the male. The data has a high statistical significance re-asserting its reliability. Thus flow cytometric analysis reveals higher QD uptake by the male salivary gland fibroblasts.

In the flow cytometry data of tumor cells shown by 4.6, we see a relatively lower nanoparticle uptake by the cells as compared to the QD uptake by salivary gland fibroblasts (4.1). The gastric cells showed higher intensity in forward scatter and lower in the side scatter (SSC) signal during flow run indicating that they have a granular morphology (see 6.1). Smaller granular cells are not able to take up as many particles as large cells leading to a lower overall MFI. In some studies, SSC intensity has been proven to be well correlated with the fluorescence intensity computed from dyes in both prokaryotic and eukaryotic cells [85].

The similar MFI levels of the 136T tumors and stroma (4.6) is indicative of the tumor and stromal environments having similar nanoparticle uptake capacities. The variation of particle uptake between tumors and stroma will have to be analyzed in more cell populations to determine any potential differences that would have to be incorporated into nanoparticle-based cancer therapeutics targeted against the tumor microenvironment. We will need more representative experiments on tumor cells to detect

6.1 Discussions

any significant patterns of NP uptake in cell groups.

Overall, it is noteworthy that there may be a lot of factors at play here, primarily cell type, gender, patient age, type and progression of cancer, whether the tumors have undergone EMT or not, as well as nanoparticle-based factors like size, surface functionalization, protein corona, etc.

6.1.2 Confocal Microscopy

Confocal imaging was performed using two sets of age-matched cells. From the confocal images itself (4.4) it is clear how the female cultures internalize lesser number of QDs denoted by green areas (white arrows). The endocytosis is even lesser in the females of the second set of cells (4.4D). The corresponding graphs (4.5) corroborate the results we saw from flow cytometry with the male groups showing almost double the percentage of QD uptake than females in both sets. This indicates that particle endocytosis does not differ significantly with the age of the patient. Research in age-related changes in cell cytoskeleton has mainly been attributed to microtubular alterations [86]. Therefore, we may identify actin (and/or secreted proteins) as still being the major player in regulating particle uptake in cells.

Confocal images of 136T and 181T tumors shown in 4.8 and 4.9 indicate a fibre-like network of nanoparticles which is most probably the microtubule network that particles rely on to translocate after internalization at the cell periphery to the nucleus. Studies with lesser concentrations of nanoparticles would be beneficial in obtaining more detailed information of particle internalization and translocation within cells. It would also become easier to quantify and compare nanoparticle uptake levels amongst the varying cell types.

6.1.3 Super Resolution Microscopy

It is known that actin has a critical role in controlling the localization of the endocytosis machinery to the cellular plasma membrane (e.g., the clathrin-mediated endocytosis process) and also on the

6.1 Discussions

consequent separation of the formed vesicles from the plasma membrane and on their intracellular movements. Hence, it is legitimate to expect the observed differences in organization, distribution, and morphology of actin in male and female cells could differentially affect uptake and cellular trafficking of QDs. Lu and co-workers [87] revealed that an increase in actin filament thickness can enhance the mechanical properties (e.g., stiffness) of cells. Therefore, as male and female salivary gland fibroblasts have a differing organization, distribution, and morphology of actin filaments/bundles, one would expect these cells may have different cellular stiffness, which affects membrane deformations required for endocytosis, explaining in part sex-specific uptake of QDs.

As observed in 4.1A & B, the male salivary gland fibroblasts have a higher concentration of actin fibres on the cell periphery which most probably are stress fibres. It is known that the presence of actin stress fibres near to the plasma membrane aids in membrane invagination and receptor-mediated endocytosis by budding off of the membrane during particle internalization [58].

The increased concentration of clathrin heavy chains found on the male somatic fibroblasts, which have fewer actin filaments, correlated with greater and more rapid QD uptake as seen in 5.2. The number of punctate structures (presumptive coated pits) in male cells was increased after treatment with QDs (5.2e & f) demonstrating that interaction of QDs with cells can increase the accumulation of clathrin on the cell surface. However, the results suggested that male cells have a higher accumulation of the clathrin heavy chains in punctate structures than female cells after interactions with QDs which would be a direct result of male cells internalizing relatively more number of quantum dots than female cells.

6.1.4 Transmission Electron Microscopy

The bundle of filaments seen near the top of the image (5.3 A) is most likely actin stress fibers similar to those seen in the fluorescence image (5.1). In TEM, we cannot rule out that this bundle may also contain intermediate filaments and microtubules. The TEM images (5.3 C and D) of the male cells

6.1 Discussions

show a much less dense network of actin filaments, as is also evident by the lack of diffuse fluorescent signal in the light microscopy images (5.1 A, B) of the male cells.

While clathrin-coated and other endosomal vesicles could be visualized in large numbers (5.5), only a few of the gold NPs could be visualized in endosomes or lysosomes (5.4 B); the gold NPs were found exclusively in non-coated vesicles. Thus, we could not confirm that they were brought into the cells by clathrin coated vesicles or caveolae. However, isolated or aggregated gold particles were visualized within the cytosol (5.4 A). Some of these gold NPs were associated with clathrin on the outer surface of clathrin-coated vesicles (insert A-1 in 5.5 A), consistent with the light microscopic images, but unexpectedly on the cytoplasmic side of clathrin-coated vesicles or pits. These data are consistent with endocytosis in noncoated vesicles (e.g., macropinocytosis, which is actin-mediated) or by non-endocytotic direct penetration of the plasma membrane [88]. It is likely then that association of gold particles with clathrin occurs after their entry into the cell. We also emphasize that the mechanism of entry of quantum dots could be different from that of gold NPs. More research will be required to investigate these issues. Based on TEM data there may be other differences, including changes in mitochondrial and endoplasmic reticulum structure as well, which may be the subjects of future investigation.

6.1.5 Zeta Potential Analysis and Proteomics

The commercial quantum dots purchased from Invitrogen has a cadmium sulphide core and a zinc sulphide shell functionalized with an amphiphilic polymer coating. The carboxylic groups in the polymer imparts negative charges to the nanoparticle making their surface charge negative (see Table 6.1). In the physiological environment numerous proteins interact with the NP resulting in the formation of a protein corona. This phenomenon is bound to alter the zeta potential value of the NP. As seen in Table 6.1, the surface charge of the NP increases for male and female cell supernatants and to a value even closer to zero for the co-culture supernatant.

6.1 Discussions

Table 6.1: The secreted proteins identified from the hard corona of cell samples. Mean abundance is the average of the percentage normalized spectral counts of the proteins in the male, female and co-culture coronas. Net charge for each protein is given at physiological pH=7.4.

Identified Proteins	Mean Abundance (%)	Net Charge	Isoelectric Point (pI)
Elastin	0.12	37.951	10.232
Ladinin-1	0.06	16.186	9.473
Glia-derived nexin	0.09	9.113	9.095
Collagen alpha-2(I) chain	1.28	11.753	8.755
Transgelin	0.15	2.228	8.606
Decorin	0.23	3.882	8.3
Leucine-rich repeat-containing protein 17	0.20	4.201	7.98
Insulin-like growth factor-binding protein 5	0.89	4.468	7.958
Metalloproteinase inhibitor 1	1.34	2.112	7.822
Protein-lysine 6-oxidase	0.29	2.357	7.807
Connective tissue growth factor	0.29	4.820	7.755
Transforming growth factor-beta-induced protein ig-h3	0.19	-0.088	7.385
Pyruvate kinase PKLR	0.06	-0.141	7.36
Annexin A2	0.10	-0.164	7.329
Kallistatin	3.60	-0.328	7.31
Periostin	0.13	-1.439	7.154
Insulin-like growth factor-binding protein 4	0.25	-3.698	6.763
Inter-alpha-trypsin inhibitor heavy chain H2	0.32	-7.874	6.47
Collagen alpha-1(III) chain	0.11	-9.793	6.265
Lumican	0.15	-5.141	6.227

6.1 Discussions

Hemicentin-1	0.02	-82.185	6.136
Alpha-2-macroglobulin	0.47	-24.224	6.1
Heat shock protein beta-6	0.69	-4.524	6.027
Gelsolin	0.07	-11.080	5.956
Microfibrillar-associated protein 5	0.38	-4.540	5.677
Collagen alpha-1(I) chain	1.26	-15.568	5.629
Alpha-fetoprotein	0.06	-21.872	5.514
Fibronectin	1.53	-62.191	5.501
Mucin-16	0.00	-436.686	5.154
Fibulin-1	0.12	-39.269	5.092
Fibulin-2	0.03	-87.056	4.738
Thrombospondin-1	0.63	-74.857	4.729

There are several theories of the dynamics of how proteins adsorb onto the NP surface. Some proteins adsorb as monolayers while others interact in the form of their secondary structures. In a liquid medium, proteins acquire a net charge because of their zwitterionic amino acid constituents. In case of proteins in secondary structures, the branches may be positively or negatively charged and bind to oppositely charged surfaces owing to electrostatic attractions. This concept is at play at the site of protein corona formation as well. More extensive research is required to unravel the physicochemical reactions occurring between proteins and the NP surface to elucidate how exactly it affects surface charge and subsequent endocytosis dynamics. The zeta potential of QDs incubated in male-female coculture supernatant dropped to -5 ± 3 mV, indicating paracrine signaling dependence in populations of cells derived from a single-sex source versus mixed sex cultures. As seen in 5.7, the co-culture corona encompasses a wider variety and abundance of all the proteins identified in the experiment which presumably resulted in the drastic increase in surface charge of co-culture supernatant incubated NPs.

6.1 Discussions

6.1 lists all the proteins identified in the hard protein corona of male, female and co-culture samples with their corresponding percentage abundances, net charge (at pH=7.4) and isoelectric point. All data was obtained from UniProtKB database [89].

Several studies have shown that negatively charged nanoparticles adsorb proteins with a pI greater than 5.5 [90]. This is demonstrated in Table 6.1 (proteins listed according to decreasing pI values) where all proteins except the last four (mucin-16, fibulin-1, fibulin-2, and thrombospondin-1) have pI values greater than 5.5. As the pI decreases, the net charge of the proteins does as well. It is also to be noted that most proteins are negatively charged but their relative abundances in different sex samples vary. Again, more in-depth research is required to decipher the nuances of the inter-relationship between net charge, isoelectric points, and NP surface affinity of the proteins.

6.1.6 Cell Gender Project: Collaborator's Work

Similar experiments as were done for the salivary gland fibroblasts were conducted at our collaborator's labs for the cell gender project. They used stem cells extracted from the amniotic fluid of male and female fetuses using the same quantum dot nanoparticles. Interestingly, flow cytometry and immunohistochemical imaging showed a higher accumulation of QDs in the female cells as opposed to higher abundance of the same particles in male cells in case of the salivary gland fibroblasts. Structural differences in actin filament organization between male and female cells were observed with the help of 3D super resolution microscopy. Clathrin heavy chain was found in punctate structures consistent with its expected localization in coated pits. The male cells had a higher accumulation of the clathrin heavy chains in punctate structures than female cells after interactions with QDs. In addition, correlative epifluorescence and STORM imaging suggested that clathrin punctae colocalized with some of the QDs in male cells, suggesting that uptake of those QDs occurred through clathrin-coated endocytosis. 63-Plex Luminex immunoassay of human cytokines detected significant changes in the production of 14 cytokines in the supernatant of amniotic mesenchymal stem cells extracted from the male versus

6.2 Conclusions and Future Work

female fetuses ([53]).

6.2 Conclusions and Future Work

We have seen that factors like cell gender, age of the patient, cancer invasiveness and source do affect the endocytosis of nanoparticles in primary cells. These variations can be linked to differences in the cytoskeleton of cell types that were probed using several microscopy techniques. From the experiments conducted at our collaborators' labs it is evident that the effect of cell sex varied between cell types (fibroblasts and human amniotic stem cells). Distinct differences in secreted paracrine factors were also observed in the salivary gland fibroblasts that in turn affected the composition of the respective protein coronas of the cells. More extensive proteomic studies can lead to better conclusions on the changes brought about by secreted proteins or protein profiles in blood plasmas of the patient. We also tried to establish a correlation between the uptake patterns in the tumor and stromal cultures of cancer cell populations and found no distinct differences in particle uptake levels although more populations must be tested to check for consistency of the results. Overall, we have found that there are several hidden factors and phenomena that are at play at the cell-nanoparticle interface and each of them do influence the fate of any nanoparticle-based therapeutics targeted to the specific tissue or organ.

This project needs validation studies in a wide variety of primary cells and 3D cultures which mimic the actually physiological environment on the cells even better. The cancer nanoparticle project is still underway with time and temperature-dependent uptake studies. We also intend to perform actin imaging on the tumor cells to identify significant differences in cytoskeletal organization. Repeating the uptake studies with active and passive endocytosis inhibitors would allow a clearer insight into the mechanisms involved in the same. In the near future, we plan to analyze the paracrine secretions of the cells and conduct proteomic studies on the protein coronas of NPs incubated in cell supernatant. Once again, more detailed studies on a greater variety of patients while minimizing the many variables at play is necessary to analyze the contributions of each factor individually in cell nanoparticle endocytosis.

6.2 Conclusions and Future Work

We are thus opening new realms in precision nanomedicine and personalized medicine by taking into account the effect of all these factors on the nanobio interactions to optimize clinical translation of NPs and to help researchers to better design and produce safe and efficient therapeutic NPs [4, 91, 92, 30, 93, 94, 95, 96, 97].

List of Publications

Published:

Effect of Cell Sex on Uptake of Nanoparticles: The Overlooked Factor at the Nanobio Interface

Vahid Serpooshan, Sara Sheibani, Pooja Pushparaj, Michal Wojcik, Albert Y. Jang, Michelle R. Santoso, Joyce H. Jang, Haina Huang, Reihaneh Safavi-Sohi, Niloofar Haghjoo, Hossein Nejadnik, Haniyeh Aghaverdi, Hojatollah Vali, Joseph Matthew Kinsella, John Presley, Ke Xu, Phillip Chung-Ming Yang, and Morteza Mahmoudi *ACS Nano* 2018 12 (3), 2253-2266 DOI: 10.1021/acsnano.7b06212

Author Contributions : V. Serpooshan, S. Sheibani, P. Pushparaj, M. Wojcik, and A. Y. Jang contributed equally to this work.

Co-corresponding Authors: Joseph Matthew Kinsella, John Presley, Ke Xu, Phillip Chung-Ming Yang, and Morteza Mahmoudi

Bibliography

- [1] H. R. H. Salaheldeen Elnashaie S., Danafar F., “From nanotechnology to nanoengineering,” *Springer, Singapore*, vol. 64, 2012. [1](#)
- [2] A. E. Nel, L. Mädler, D. Velegol, T. Xia, E. M. Hoek, P. Somasundaran, F. Klaessig, V. Castanova, and M. Thompson, “Understanding biophysicochemical interactions at the nano–bio interface,” *Nature materials*, vol. 8, no. 7, p. 543, 2009. [1](#), [1.2](#)
- [3] W. Jing, Q. WaseemAkthar, L. Yiye, X. Jianxun, and N. Guangjun, “Analytical methods for nano-bio interface interactions,” *SCIENCE CHINA Chemistry*, vol. 59, no. 11, pp. 1467–1478, 2016. [1](#)
- [4] M. Mahmoudi, A. M. Abdelmonem, S. Behzadi, J. H. Clement, S. Dutz, M. R. Ejtehad, R. Hartmann, K. Kantner, U. Linne, P. Maffre, S. Metzler, M. K. Moghadam, C. Pfeiffer, M. Rezaei, P. Ruiz-Lozano, V. Serpooshan, M. A. Shokrgozar, G. U. Nienhaus, and W. J. Parak, “Temperature: The ignored factor at the nanobio interface,” *ACS Nano*, vol. 7, no. 8, pp. 6555–6562, 2013. PMID: 23808533. [1](#), [1.2](#), [6.2](#)
- [5] X.-Q. Zhang, X. Xu, N. Bertrand, E. Pridgen, A. Swami, and O. C. Farokhzad, “Interactions of nanomaterials and biological systems: Implications to personalized nanomedicine,” vol. 64, no. 13, pp. 1363–1384, 2012. Exported from <https://app.dimensions.ai> on 2018/08/15. [1](#)
- [6] O. N. Oliveira, R. M. Iost, J. R. Siqueira, F. N. Crespilho, and L. Caseli, “Nanomaterials for diagnosis: Challenges and applications in smart devices based on molecular recognition,” *ACS Applied Materials & Interfaces*, vol. 6, no. 17, pp. 14745–14766, 2014. PMID: 24968359. [1.1](#)

BIBLIOGRAPHY

- [7] D. P. Cormode, P. C. Naha, and Z. A. Fayad, “Nanoparticle contrast agents for computed tomography: A focus on micelles,” *Contrast Media Mol Imaging*, vol. 9, pp. 37–52, Jan 2014. 24470293[pmid]. 1.1
- [8] L. Lan, Y. Yao, J. Ping, and Y. Ying, “Recent advances in nanomaterial-based biosensors for antibiotics detection,” *Biosensors and Bioelectronics*, vol. 91, pp. 504 – 514, 2017. 1.1
- [9] A. Alsaiee, R. Beingessner, and H. Fenniri, “17 - self-assembled nanomaterials for tissue-engineering applications,” in *Nanomedicine* (T. J. Webster, ed.), Woodhead Publishing Series in Biomaterials, pp. 490 – 533, Woodhead Publishing, 2012. 1.1
- [10] W. H. De Jong and P. J. Borm, “Drug delivery and nanoparticles: Applications and hazards,” *Int J Nanomedicine*, vol. 3, pp. 133–149, Jun 2008. 18686775[pmid]. 1.1
- [11] K. M. Abu-Salah, S. A. Alrokyan, M. N. Khan, and A. A. Ansari, “Nanomaterials as analytical tools for genosensors,” *Sensors (Basel)*, vol. 10, pp. 963–993, Jan 2010. sensors-10-00963[PII]. 1.1
- [12] C. L. Ventola, “The nanomedicine revolution: Part 1: Emerging concepts,” *P T*, vol. 37, pp. 512–525, Sep 2012. ptj3709512[PII]. 1.1
- [13] “Market report on emerging nanotechnology now available,” Last accessed 2018. National Science Foundation - Media Advisory 14-004. 1.1
- [14] F. Franconi, S. Brunelleschi, L. Steardo, and V. Cuomo, “Gender differences in drug responses,” *Pharmacological Research*, vol. 55, no. 2, pp. 81 – 95, 2007. 1.1
- [15] R. Hodson, “Precision medicine,” *Nature*, vol. 537, pp. S49 EP –, Sep 2016. 1.1
- [16] M. Bar-Zeev, Y. D. Livney, and Y. G. Assaraf, “Targeted nanomedicine for cancer therapeutics: Towards precision medicine overcoming drug resistance,” *Drug Resistance Updates*, vol. 31, pp. 15–30, 2017. 1.1

BIBLIOGRAPHY

- [17] P. V. Baptista, “Precision nanomedicine in cancer: how far are we from personalization?,” *Expert Review of Precision Medicine and Drug Development*, vol. 1, no. 3, pp. 227–228, 2016. [1.1](#)
- [18] Y. F. Tan, L. L. Lao, G. M. Xiong, and S. Venkatraman, “Controlled-release nanotherapeutics: State of translation,” *Journal of Controlled Release*, vol. 284, pp. 39 – 48, 2018. [1.1](#)
- [19] M. Mahmoudi, N. Bertrand, H. Zope, and O. C. Farokhzad, “Emerging understanding of the protein corona at the nano-bio interfaces,” *Nano Today*, vol. 11, no. 6, pp. 817 – 832, 2016. [1.2](#)
- [20] M. Mahmoudi, H. Hofmann, B. Rothen-Rutishauser, and A. Petri-Fink, “Assessing the in vitro and in vivo toxicity of superparamagnetic iron oxide nanoparticles,” *Chemical Reviews*, vol. 112, no. 4, pp. 2323–2338, 2012. PMID: 22216932. [1.2](#)
- [21] L. T. Nguyen, A. Muktabar, J. Tang, V. P. Dravid, C. S. Thaxton, S. Venkatraman, and K. W. Ng, “Engineered nanoparticles for the detection, treatment and prevention of atherosclerosis: how close are we?,” *Drug discovery today*, vol. 22, no. 9, pp. 1438–1446, 2017. [1.3](#)
- [22] B. B. S. Cerqueira, A. Lasham, A. N. Shelling, and R. Al-Kassas, “Nanoparticle therapeutics: Technologies and methods for overcoming cancer,” *European Journal of Pharmaceutics and Biopharmaceutics*, vol. 97, pp. 140–151, 2015. [1.3](#)
- [23] C. Y. Wong, H. Al-Salami, and C. R. Dass, “Potential of insulin nanoparticle formulations for oral delivery and diabetes treatment,” *Journal of Controlled Release*, vol. 264, pp. 247–275, 2017. [1.3](#)
- [24] U. Prabhakar, H. Maeda, R. K. Jain, E. M. Sevick-Muraca, W. Zamboni, O. C. Farokhzad, S. T. Barry, A. Gabizon, P. Grodzinski, and D. C. Blakey, “Challenges and key considerations of the enhanced permeability and retention effect for nanomedicine drug delivery in oncology,” *Cancer Research*, vol. 73, no. 8, pp. 2412–2417, 2013. [1.3](#)

BIBLIOGRAPHY

- [25] T. Andreani, P. Severino, L. M. de Hollanda, M. Vazzana, S. B. Souto, A. Santini, A. M. Silva, and E. B. Souto, “Cancer therapies: applications, nanomedicines and nanotoxicology,” in *Nanostuctures for Cancer Therapy*, pp. 241–260, Elsevier, 2017. 1.3
- [26] C. M. Beddoes, C. P. Case, and W. H. Briscoe, “Understanding nanoparticle cellular entry: a physicochemical perspective,” *Advances in colloid and interface science*, vol. 218, pp. 48–68, 2015. 1.3, 1.4
- [27] M. Mahmoudi, “Debugging nano-bio interfaces: Systematic strategies to accelerate clinical translation of nanotechnologies,” *Trends in biotechnology*, 2018. 1.3
- [28] V. Mirshafiee, R. Kim, S. Park, M. Mahmoudi, and M. L. Kraft, “Impact of protein pre-coating on the protein corona composition and nanoparticle cellular uptake,” *Biomaterials*, vol. 75, pp. 295–304, 2016. 1.3
- [29] G. Caracciolo, “Liposome–protein corona in a physiological environment: challenges and opportunities for targeted delivery of nanomedicines,” *Nanomedicine: Nanotechnology, Biology and Medicine*, vol. 11, no. 3, pp. 543–557, 2015. 1.3
- [30] M. J. Hajipour, S. Laurent, A. Aghaie, F. Rezaee, and M. Mahmoudi, “Personalized protein coronas: a key factor at the nanobiointerface,” *Biomaterials Science*, vol. 2, no. 9, pp. 1210–1221, 2014. 1.3, 6.2
- [31] Z. Chu, Y. Huang, Q. Tao, and Q. Li, “Cellular uptake, evolution, and excretion of silica nanoparticles in human cells,” *Nanoscale*, vol. 3, no. 8, pp. 3291–3299, 2011. 1.4
- [32] B. D. Chithrani and W. C. Chan, “Elucidating the mechanism of cellular uptake and removal of protein-coated gold nanoparticles of different sizes and shapes,” *Nano letters*, vol. 7, no. 6, pp. 1542–1550, 2007. 1.4

BIBLIOGRAPHY

- [33] B. D. Chithrani, A. A. Ghazani, and W. C. Chan, “Determining the size and shape dependence of gold nanoparticle uptake into mammalian cells,” *Nano letters*, vol. 6, no. 4, pp. 662–668, 2006. 1.4
- [34] J. Kim, J. C. Sunshine, and J. J. Green, “Differential polymer structure tunes mechanism of cellular uptake and transfection routes of poly (β -amino ester) polyplexes in human breast cancer cells,” *Bioconjugate chemistry*, vol. 25, no. 1, pp. 43–51, 2013. 1.4
- [35] S. Salatin and A. Yari Khosroushahi, “Overviews on the cellular uptake mechanism of polysaccharide colloidal nanoparticles,” *Journal of Cellular and Molecular Medicine*, vol. 21, no. 9, pp. 1668–1686. 1.4
- [36] J. A. Swanson, “Shaping cups into phagosomes and macropinosomes,” *Nature Reviews Molecular Cell Biology*, vol. 9, 07 2008. 1.4
- [37] A. Banerjee, A. Berezhkovskii, and R. Nossal, “Kinetics of cellular uptake of viruses and nanoparticles via clathrin-mediated endocytosis,” *Physical biology*, vol. 13, no. 1, p. 016005, 2016. 1.4
- [38] W.-L. L. Suen and Y. Chau, “Size-dependent internalisation of folate-decorated nanoparticles via the pathways of clathrin and caveolae-mediated endocytosis in arpe-19 cells,” *Journal of Pharmacy and Pharmacology*, vol. 66, no. 4, pp. 564–573. 1.4
- [39] C. Dalal, A. Saha, and N. R. Jana, “Nanoparticle multivalency directed shifting of cellular uptake mechanism,” *The Journal of Physical Chemistry C*, vol. 120, no. 12, pp. 6778–6786, 2016. 1.4
- [40] R. B. Selvi, S. Chatterjee, D. Jagadeesan, P. Chaturbedy, B. S. Suma, M. Eswaramoorthy, and T. K. Kundu, “Atp driven clathrin dependent entry of carbon nanospheres prefer cells with glucose receptors,” *Journal of Nanobiotechnology*, vol. 10, p. 35, Aug 2012. 1.4

BIBLIOGRAPHY

- [41] J. Rappoport, “Focusing on clathrin-mediated endocytosis,” *Biochemical Journal*, vol. 412, pp. 415–423, 6 2008. 1.4
- [42] T. J. Pucadyil and S. L. Schmid, “Conserved functions of membrane active gtpases in coated vesicle formation,” *Science*, vol. 325, no. 5945, pp. 1217–1220, 2009. 1.4
- [43] L. Kou, J. Sun, Y. Zhai, and Z. He, “The endocytosis and intracellular fate of nanomedicines: Implication for rational design,” *Asian Journal of Pharmaceutical Sciences*, vol. 8, no. 1, pp. 1–10, 2013. 1.4
- [44] N. Malod-Dognin, J. Petschnigg, and N. PrÅžulj, “Precision medicine â a promising, yet challenging road lies ahead,” *Current Opinion in Systems Biology*, vol. 7, pp. 1 – 7, 2018. â Future of systems biologyâ Genomics and epigenomics. 1.5
- [45] L. Gaignebet and G. Kararigas, “En route to precision medicine through the integration of biological sex into pharmacogenomics,” *Clinical Science*, vol. 131, no. 4, pp. 329–342, 2017. 1.5
- [46] V. Regitz-Zagrosek, *Sex and Gender Differences in Cardiovascular Disease*, pp. 17–44. London: Springer London, 2012. 1.5, 1.5.1
- [47] F. Mauvais-Jarvis, “Gender differences in glucose homeostasis and diabetes,” *Physiology Behavior*, vol. 187, pp. 20 – 23, 2018. The Proceedings of the American University Symposium on Sex Differences: from Neuroscience to the Clinic and Beyond. 1.5
- [48] S. Ngo, F. Steyn, and P. McCombe, “Gender differences in autoimmune disease,” *Frontiers in Neuroendocrinology*, vol. 35, no. 3, pp. 347 – 369, 2014. Sex Differences in Neurological and Psychiatric Disorders. 1.5
- [49] H. Dao Jr and R. A. Kazin, “Gender differences in skin: a review of the literature,” *Gender medicine*, vol. 4, no. 4, pp. 308–328, 2007. 1.5

BIBLIOGRAPHY

- [50] N. A. Bradbury, “All cells have a sex: Studies of sex chromosome function at the cellular level,” in *Principles of Gender-Specific Medicine (Third Edition)*, pp. 269–290, Elsevier, 2017. 1.5.1
- [51] M. Nikezic-Ardolic, L. Lin, M. Milcevic, and Z. Zakeri, “Gender differences in cellular response,” *Lupus*, vol. 8, no. 5, pp. 375–379, 1999. PMID: 10455516. 1.5.1
- [52] C. Zeller, Y. Wang, T. Markel, B. Weil, A. Abarbanell, J. Herrmann, M. Kelly, A. Coffey, and D. Meldrum, “Role of tumor necrosis factor receptor 1 in sex differences of stem cell mediated cardioprotection,” *Annals of Thoracic Surgery*, vol. 87, pp. 812–819, 3 2009. 1.5.1
- [53] V. Serpooshan, S. Sheibani, P. Pushparaj, M. Wojcik, A. Y. Jang, M. R. Santoso, J. H. Jang, H. Huang, R. Safavi-Sohi, N. Haghjoo, H. Nejadnik, H. Aghaverdi, H. Vali, J. M. Kinsella, J. Presley, K. Xu, P. C.-M. Yang, and M. Mahmoudi, “Effect of cell sex on uptake of nanoparticles: The overlooked factor at the nanobio interface,” *ACS nano*, vol. 12, pp. 2253–2266, March 2018. 1.5.1, 6.1.6
- [54] J. Klingström, T. Lindgren, and C. Ahlm, “Sex-dependent differences in plasma cytokine responses to hantavirus infection,” *Clinical and Vaccine Immunology*, vol. 15, no. 5, pp. 885–887, 2008. 1.5.1
- [55] D. Furman, B. P. Hejblum, N. Simon, V. Jojic, C. L. Dekker, R. Thiébaud, R. J. Tibshirani, and M. M. Davis, “Systems analysis of sex differences reveals an immunosuppressive role for testosterone in the response to influenza vaccination,” *Proceedings of the National Academy of Sciences*, vol. 111, no. 2, pp. 869–874, 2014. 1.5.1
- [56] A. Adamek, A. Kasprzak, A. Seraszek, H. Mikoś, A. Bura, and I. Mozer-Lisewska, “Alterations of insulin-like growth factor i (igf-i) and estradiol serum levels in chronic hepatitis c,” *Contemporary oncology*, vol. 16, no. 3, p. 234, 2012. 1.5.1
- [57] M. J. Iglesias, S. Eiras, R. Piñeiro, D. López-Otero, R. Gallego, Á. L. Fernández, F. Lago, and J. R. González-Juanatey, “Gender differences in adiponectin and leptin expression in epicardial and

BIBLIOGRAPHY

- subcutaneous adipose tissue. findings in patients undergoing cardiac surgery,” *Revista Española de Cardiología (English Edition)*, vol. 59, no. 12, pp. 1252–1260, 2006. [1.5.1](#)
- [58] B. Qualmann, M. M. Kessels, and R. B. Kelly, “Molecular links between endocytosis and the actin cytoskeleton,” *The Journal of Cell Biology*, vol. 150, pp. 111–116, 09 2000. [1.5.2](#), [6.1.3](#)
- [59] L. C. Boraas, J. B. Guidry, E. T. Pineda, and T. Ahsan, “Cytoskeletal expression and remodeling in pluripotent stem cells,” *PloS one*, vol. 11, no. 1, p. e0145084, 2016. [1.5.2](#)
- [60] D. Höfer, D.-W. Shin, and D. Drenckhahn, “Identification of cytoskeletal markers for the different microvilli and cell types of the rat vomeronasal sensory epithelium,” *Journal of neurocytology*, vol. 29, no. 3, pp. 147–156, 2000. [1.5.2](#)
- [61] E. Rungger-Brändle, T. Achtstätter, and W. W. Franke, “An epithelium-type cytoskeleton in a glial cell: astrocytes of amphibian optic nerves contain cytokeratin filaments and are connected by desmosomes.,” *The Journal of Cell Biology*, vol. 109, no. 2, pp. 705–716, 1989. [1.5.2](#)
- [62] P. Bannasch, H. Zerban, and D. Mayer, “The cytoskeleton in tumor cells,” *Pathology - Research and Practice*, vol. 175, no. 2, pp. 196 – 211, 1982. [1.6](#)
- [63] H. L. Malech and T. L. Lentz, “Microfilaments in epidermal cancer cells,” vol. 60, no. 2, pp. 473–482, 1974. [1.6](#)
- [64] P. Z. K. Schenk, “Microfilaments in human epithelial cancer cells,” vol. 84, no. 241, pp. 1432–1335, 1975. [1.6](#)
- [65] B. H. Toh and H. K. Muller, “Smooth muscle-associated antigen in experimental cutaneous squamous cell carcinoma, keratoacanthoma, and papilloma,” *Cancer Research*, vol. 35, no. 12, pp. 3741–3745, 1975. [1.6](#)

BIBLIOGRAPHY

- [66] N. McNutt, "Ultrastructural comparison of the interface between epithelium and stroma in basal cell carcinoma and control human skin," *Laboratory investigation; a journal of technical methods and pathology*, vol. 35, p. 132â142, August 1976. 1.6
- [67] B. Toh, G. Hard, M. Cauchi, and H. Muller, "Smooth-muscle-associated contractile protein in renal mesenchymal tumour cells and in transformed cells from dmn-injected rats," *British journal of cancer*, vol. 34, no. 5, p. 533, 1976. 1.6
- [68] G. C. Hard and B. Toh, "Immunofluorescent characterization of rat kidney tumors according to the distribution of actin as revealed by specific antiactin antibody," *Cancer research*, vol. 37, no. 6, pp. 1618–1623, 1977. 1.6
- [69] J. C. Macartney, J. Roxburgh, and R. C. Curran, "Intracellular filaments in human cancer cells: A histological study," *The Journal of Pathology*, vol. 129, no. 1, pp. 13–20. 1.6
- [70] A. Raz and B. Geiger, "Altered organization of cell-substrate contacts and membrane-associated cytoskeleton in tumor cell variants exhibiting different metastatic capabilities," *Cancer Research*, vol. 42, no. 12, pp. 5183–5190, 1982. 1.6
- [71] B. SUN, Y. FANG, Z. LI, Z. CHEN, and J. XIANG, "Role of cellular cytoskeleton in epithelial-mesenchymal transition process during cancer progression," *Biomed Rep*, vol. 3, pp. 603–610, Sep 2015. BR-0-0-494[PII]. 1.6
- [72] J. Shankar and I. R. Nabi, "Actin cytoskeleton regulation of epithelial mesenchymal transition in metastatic cancer cells," *PLOS ONE*, vol. 10, pp. 1–12, 03 2015. 1.6
- [73] D. Yao, C. Dai, and S. Peng, "Mechanism of mesenchymal-epithelial transition and the relationship with metastatic tumor formation," *Molecular cancer research*, pp. molcanres–0568, 2011. 1.6

BIBLIOGRAPHY

- [74] N. Oh and J.-H. Park, “Endocytosis and exocytosis of nanoparticles in mammalian cells,” *Int J Nanomedicine*, vol. 9, pp. 51–63, May 2014. [ijn-9-051\[PII\]](#). [1.6](#)
- [75] V. H. Nguyen and B.-J. Lee, “Protein corona: a new approach for nanomedicine design,” *Int J Nanomedicine*, vol. 12, pp. 3137–3151, Apr 2017. [ijn-12-3137\[PII\]](#). [1.6](#)
- [76] M. Mettlen and G. Danuser, “Imaging and modeling the dynamics of clathrin-mediated endocytosis,” *Cold Spring Harbor Perspectives in Biology*, vol. 6, no. 12, 2014. [3.1](#)
- [77] N. Hondow, R. Brydson, and A. Brown, “The use of transmission electron microscopy in the quantification of nanoparticle dose,” *Journal of Physics: Conference Series*, vol. 522, no. 1, p. 012055, 2014. [3.1](#)
- [78] R. Lévy, U. Shaheen, Y. Cesbron, and V. Sée, “Gold nanoparticles delivery in mammalian live cells: a critical review,” *Nano Reviews*, vol. 1, p. 10.3402/nano.v1i0.4889, 2010. [3.1](#), [5.1.2](#)
- [79] E. Fröhlich, “The role of surface charge in cellular uptake and cytotoxicity of medical nanoparticles,” *International Journal of Nanomedicine*, vol. 7, pp. 5577–5591, 2012. [3.1](#)
- [80] S.-H. Lee, J. Y. Shin, A. Lee, and C. Bustamante, “Counting single photoactivatable fluorescent molecules by photoactivated localization microscopy (palm),” *Proceedings of the National Academy of Sciences*, vol. 109, no. 43, pp. 17436–17441, 2012. [3.1](#)
- [81] J. B. Harford, “Preparation and isolation of cells,” *Current Protocols in Cell Biology*, vol. 32, no. 1, pp. 2.0.1–2.0.2. [3.1.2.1](#)
- [82] M. J. Rust, M. Bates, and X. Zhuang, “Stochastic optical reconstruction microscopy (storm) provides sub-diffraction-limit image resolution,” *Nature methods*, vol. 3, pp. 793–795, 10 2006. [3.1.2.8](#)

BIBLIOGRAPHY

- [83] B. Huang, W. Wang, M. Bates, and X. Zhuang, “Three-dimensional super-resolution imaging by stochastic optical reconstruction microscopy,” *Science (New York, N.Y.)*, vol. 319, pp. 810–813, 02 2008. [3.1.2.8](#)
- [84] C. C. Valley, S. Liu, D. S. Lidke, and K. A. Lidke, “Sequential superresolution imaging of multiple targets using a single fluorophore,” *PLOS ONE*, vol. 10, pp. 1–22, 04 2015. [3.1.2.8](#)
- [85] A. Tzur, J. K. Moore, P. Jorgensen, H. M. Shapiro, and M. W. Kirschner, “Optimizing optical flow cytometry for cell volume-based sorting and analysis,” *PLOS ONE*, vol. 6, pp. 1–9, 01 2011. [6.1.1](#)
- [86] K. Rao and H. Cohen, “Actin cytoskeletal network in aging and cancer,” *Mutation research*, vol. 256, no. 2-6, p. 139–148, 1991. [6.1.2](#)
- [87] L. Lu, S. J. Oswald, H. Ngu, and F. C.-P. Yin, “Mechanical properties of actin stress fibers in living cells,” *Biophysical Journal*, vol. 95, pp. 6060–6071, 12 2008. [6.1.3](#)
- [88] S. Behzadi, V. Serpooshan, W. Tao, M. A. Hamaly, M. Y. Alkawareek, E. C. Dreaden, D. Brown, A. M. Alkilany, O. C. Farokhzad, and M. Mahmoudi, “Cellular uptake of nanoparticles: Journey inside the cell,” *Chemical Society reviews*, vol. 46, pp. 4218–4244, 07 2017. [6.1.4](#)
- [89] C. Chen, H. Huang, and C. H. Wu, “Protein bioinformatics databases and resources,” *Methods Mol Biol*, vol. 1558, pp. 3–39, 2017. 28150231[pmid]. [6.1.5](#)
- [90] P. Aggarwal, J. B. Hall, C. B. McLeland, M. A. Dobrovolskaia, and S. E. McNeil, “Nanoparticle interaction with plasma proteins as it relates to particle biodistribution, biocompatibility and therapeutic efficacy,” *Advanced Drug Delivery Reviews*, vol. 61, no. 6, pp. 428 – 437, 2009. Identifying and Assessing Biomaterial Nanotoxicity in Translational Research for Preclinical Drug Development. [6.1.5](#)

BIBLIOGRAPHY

- [91] M. Mahmoudi, S. E. Lohse, C. J. Murphy, A. Fathizadeh, A. Montazeri, and K. S. Suslick, “Variation of protein corona composition of gold nanoparticles following plasmonic heating,” *Nano letters*, vol. 14, no. 1, pp. 6–12, 2013. 6.2
- [92] M. J. Hajipour, J. Raheb, O. Akhavan, S. Arjmand, O. Mashinchian, M. Rahman, M. Abdollahad, V. Serpooshan, S. Laurent, and M. Mahmoudi, “Personalized disease-specific protein corona influences the therapeutic impact of graphene oxide,” *Nanoscale*, vol. 7, no. 19, pp. 8978–8994, 2015. 6.2
- [93] M. Mahmoudi, A. Simchi, M. Imani, M. A. Shokrgozar, A. S. Milani, U. O. Häfeli, and P. Stroeve, “A new approach for the in vitro identification of the cytotoxicity of superparamagnetic iron oxide nanoparticles,” *Colloids and Surfaces B: Biointerfaces*, vol. 75, no. 1, pp. 300–309, 2010. 6.2
- [94] M. Mahmoudi, M. P. Monopoli, M. Rezaei, I. Lynch, F. Bertoli, J. J. McManus, and K. A. Dawson, “The protein corona mediates the impact of nanomaterials and slows amyloid beta fibrillation,” *ChemBioChem*, vol. 14, no. 5, pp. 568–572, 2013. 6.2
- [95] G. Caracciolo, O. C. Farokhzad, and M. Mahmoudi, “Biological identity of nanoparticles in vivo: clinical implications of the protein corona,” *Trends in biotechnology*, vol. 35, no. 3, pp. 257–264, 2017. 6.2
- [96] H. Amiri, L. Bordonali, A. Lascialfari, S. Wan, M. P. Monopoli, I. Lynch, S. Laurent, and M. Mahmoudi, “Protein corona affects the relaxivity and mri contrast efficiency of magnetic nanoparticles,” *Nanoscale*, vol. 5, no. 18, pp. 8656–8665, 2013. 6.2
- [97] M. Mahmoudi, M. Yu, V. Serpooshan, J. C. Wu, R. Langer, R. T. Lee, J. M. Karp, and O. C. Farokhzad, “Multiscale technologies for treatment of ischemic cardiomyopathy,” *Nature nanotechnology*, vol. 12, no. 9, p. 845, 2017. 6.2



RightsLink®

[Home](#)[Create Account](#)[Help](#)

ACS Publications
Most Trusted. Most Cited. Most Read.

Title: Effect of Cell Sex on Uptake of Nanoparticles: The Overlooked Factor at the Nanobio Interface

Author: Vahid Serpooshan, Sara Sheibani, Pooja Pushparaj, et al

Publication: ACS Nano

Publisher: American Chemical Society

Date: Mar 1, 2018

Copyright © 2018, American Chemical Society

LOGIN

If you're a **copyright.com user**, you can login to RightsLink using your copyright.com credentials.

Already a **RightsLink user** or want to [learn more?](#)

PERMISSION/LICENSE IS GRANTED FOR YOUR ORDER AT NO CHARGE

This type of permission/license, instead of the standard Terms & Conditions, is sent to you because no fee is being charged for your order. Please note the following:

- Permission is granted for your request in both print and electronic formats, and translations.
- If figures and/or tables were requested, they may be adapted or used in part.
- Please print this page for your records and send a copy of it to your publisher/graduate school.
- Appropriate credit for the requested material should be given as follows: "Reprinted (adapted) with permission from (COMPLETE REFERENCE CITATION). Copyright (YEAR) American Chemical Society." Insert appropriate information in place of the capitalized words.
- One-time permission is granted only for the use specified in your request. No additional uses are granted (such as derivative works or other editions). For any other uses, please submit a new request.

[BACK](#)[CLOSE WINDOW](#)

Copyright © 2018 [Copyright Clearance Center, Inc.](#) All Rights Reserved. [Privacy statement.](#) [Terms and Conditions.](#)
Comments? We would like to hear from you. E-mail us at customercare@copyright.com